

# Perfluorocyclobutane (PFC-318, $c\text{-C}_4\text{F}_8$ ) in the global atmosphere

Jens Mühle<sup>1</sup>, Cathy M. Trudinger<sup>2</sup>, Luke M. Western<sup>3</sup>, Matthew Rigby<sup>3</sup>, Martin K. Vollmer<sup>4</sup>, Sunyoung Park<sup>5</sup>, Alistair J. Manning<sup>6</sup>, Daniel Say<sup>3</sup>, Anita Ganesan<sup>7</sup>, L. Paul Steele<sup>2</sup>, Diane J. Ivy<sup>8</sup>, Tim Arnold<sup>9,10</sup>, Shanlan Li<sup>5</sup>, Andreas Stohl<sup>11</sup>, Christina M. Harth<sup>1</sup>, Peter K. Salameh<sup>1</sup>, Archie McCulloch<sup>3</sup>, Simon O'Doherty<sup>3</sup>, Mi-Kyung Park<sup>5</sup>, Chun Ok Jo<sup>5</sup>, Dickon Young<sup>3</sup>, Kieran M. Stanley<sup>3</sup>, Paul B. Krummel<sup>2</sup>, Blagoj Mitrevski<sup>2</sup>, Ove Hermansen<sup>11</sup>, Chris Lunder<sup>11</sup>, Nikolaos Evangeliou<sup>11</sup>, Bo Yao<sup>12</sup>, Jooil Kim<sup>1</sup>, Benjamin Hmiel<sup>13</sup>, Christo Buizert<sup>14</sup>, Vasilii V. Petrenko<sup>13</sup>, Jgor Arduini<sup>15,16</sup>, Michela Maione<sup>15,16</sup>, David M. Etheridge<sup>2</sup>, Eleni Michalopoulou<sup>3</sup>, Mike Czerniak<sup>17</sup>, Jeffrey P. Severinghaus<sup>1</sup>, Stefan Reimann<sup>4</sup>, Peter G. Simmonds<sup>3</sup>, Paul J. Fraser<sup>2</sup>, Ronald G. Prinn<sup>8</sup>, and Ray F. Weiss<sup>1</sup>

<sup>1</sup>Scripps Institution of Oceanography, University of California, San Diego, La Jolla, CA, USA

<sup>2</sup>Climate Science Centre, CSIRO Oceans and Atmosphere, Aspendale, Victoria, Australia

<sup>3</sup>School of Chemistry, University of Bristol, Bristol, UK

<sup>4</sup>Laboratory for Air Pollution and Environmental Technology, Empa, Swiss Federal Laboratories for Materials Science and Technology, Dübendorf, Switzerland

<sup>5</sup>KNU, Kyungpook Institute of Oceanography, College of Natural Sciences, Kyungpook National University, South Korea

<sup>6</sup>Met Office Hadley Centre, Exeter, UK

<sup>7</sup>School of Geographical Sciences, University of Bristol, Bristol, UK

<sup>8</sup>Center for Global Change Science, Massachusetts Institute of Technology, Cambridge, MA, USA

<sup>9</sup>National Physical Laboratory, Teddington, Middlesex, UK

<sup>10</sup>School of GeoSciences, University of Edinburgh, Edinburgh, UK

<sup>11</sup>NILU, Norwegian Institute for Air Research, Kjeller, Norway

<sup>12</sup>Meteorological Observation Centre (MOC), China Meteorological Administration (CMA), Beijing, China

<sup>13</sup>Department of Earth & Environmental Sciences, University of Rochester, Rochester, NY, USA

<sup>14</sup>College of Earth, Ocean, and Atmospheric Sciences, Oregon State University, Corvallis, OR, USA

<sup>15</sup>Department of Pure and Applied Sciences, University of Urbino, Urbino, Italy

<sup>16</sup>ISAC-CNR, Bologna, Italy

<sup>17</sup>Edwards LTD, Burgess Hill, West Sussex, UK

*Correspondence to:* Jens Mühle (jmuhle@ucsd.edu)

Atmospheric Chemistry and Physics, acp-2019-267

37 **Abstract.** We reconstruct atmospheric abundances of the potent greenhouse gas *c*-C<sub>4</sub>F<sub>8</sub> (perfluorocyclobutane,  
38 perfluorocarbon PFC-318) from measurements of in situ, archived, firn, and aircraft air samples with precisions of  
39 ~1–2 % reported on the SIO-14 gravimetric calibration scale. Combined with inverse methods, we found near zero  
40 atmospheric abundances from the early 1900s to the early 1960s, after which they rose sharply, reaching 1.66 ppt  
41 (parts per trillion dry-air mole fraction) in 2017. Global *c*-C<sub>4</sub>F<sub>8</sub> emissions rose from near zero in the 1960s to  $1.2 \pm$   
42  $0.1$  ( $1\sigma$ ) Gg yr<sup>-1</sup> in the late 1970s to late 1980s, then declined to  $0.77 \pm 0.03$  Gg yr<sup>-1</sup> in the mid-1990s to early 2000s,  
43 followed by a rise since the early 2000s to  $2.20 \pm 0.05$  Gg yr<sup>-1</sup> in 2017. These emissions are significantly larger than  
44 inventory-based emission estimates. Estimated emissions from eastern Asia rose from 0.36 Gg yr<sup>-1</sup> in 2010 to 0.73  
45 Gg yr<sup>-1</sup> in 2016 and 2017, 31 % of global emissions, mostly from eastern China. We estimate emissions of 0.14 Gg  
46 yr<sup>-1</sup> from Northern and Central India in 2016 and find evidence for significant emissions from Russia. In contrast,  
47 recent emissions from North Western Europe and Australia are estimated to be small ( $\leq 1$  % each). We suggest that  
48 emissions from China, India and Russia are likely related to production of polytetrafluoroethylene (PTFE, “Teflon”)  
49 and other fluoropolymers and fluorochemicals that are based on the pyrolysis of hydrochlorofluorocarbon HCFC-22  
50 (CHClF<sub>2</sub>) in which *c*-C<sub>4</sub>F<sub>8</sub> is a known by-product. The semiconductor sector, where *c*-C<sub>4</sub>F<sub>8</sub> is used, is estimated to be  
51 a small source, at least in South Korea, Japan, Taiwan, and Europe. Without an obvious correlation with population  
52 density, incineration of waste containing fluoropolymers is probably a minor source, and we find no evidence of  
53 emissions from electrolytic production of aluminum in Australia. While many possible emissive uses of *c*-C<sub>4</sub>F<sub>8</sub> are  
54 known and though we cannot categorically exclude unknown sources, the start of significant emissions may well be  
55 related to the advent of commercial PTFE production in 1947. Process controls or abatement to reduce *c*-C<sub>4</sub>F<sub>8</sub> by-  
56 product were probably not in place in the early decades, explaining the increase in emissions in the 1960s/70s. With  
57 the advent of by-product reporting requirements to the United Nations Framework Convention on Climate Change  
58 (UNFCCC) in the 1990s, concern about climate change and product stewardship, abatement, and perhaps the  
59 collection of *c*-C<sub>4</sub>F<sub>8</sub> by-product for use in the semiconductor industry where it can be easily abated, it is conceivable  
60 that emissions in developed countries were stabilized and then reduced, explaining the observed emission reduction  
61 in the 1980s and 1990s. Concurrently, production of PTFE in China began to increase rapidly. Without emission  
62 reduction requirements, it is plausible that global emissions today are dominated by China and other developing  
63 countries. We predict that *c*-C<sub>4</sub>F<sub>8</sub> emissions will continue to rise and that *c*-C<sub>4</sub>F<sub>8</sub> will become the second most  
64 important emitted PFC in terms of CO<sub>2</sub>-equivalent emissions within a year or two. The 2017 radiative forcing of *c*-  
65 C<sub>4</sub>F<sub>8</sub> ( $0.52 \text{ mW m}^{-2}$ ) is small but emissions of *c*-C<sub>4</sub>F<sub>8</sub> and other PFCs, due to their very long atmospheric lifetimes,  
66 essentially permanently alter Earth’s radiative budget and should be reduced. Significant emissions inferred outside  
67 of the investigated regions clearly show that observational capabilities and reporting requirements need to be  
68 improved to understand global and country-scale emissions of PFCs and other synthetic greenhouse gases and ozone  
69 depleting substances.

70

## 71 **1 Introduction**

72 The perfluorocarbon (PFC) perfluorocyclobutane (*c*-C<sub>4</sub>F<sub>8</sub>, PFC-318, octafluorocyclobutane, CAS 115-25-3) is a very  
73 long-lived and potent greenhouse gas (GHG) regulated under the Paris Agreement of the United Nations Framework  
74 Convention on Climate Change (UNFCCC). Ravishankara et al. (1993) concluded that the most important  
75 atmospheric loss process of *c*-C<sub>4</sub>F<sub>8</sub> is Lyman- $\alpha$  photolysis resulting in an atmospheric lifetime of 3200 years. Later,  
76 Morris et al. (1995) argued that if reactions of *c*-C<sub>4</sub>F<sub>8</sub> with electrons and positive ions in the mesosphere and aloft are  
77 irreversible, the lifetime could be reduced to 1400 years, which, on human timescales, is still essentially infinite. *c*-  
78 C<sub>4</sub>F<sub>8</sub> has a radiative efficiency of 0.32 W m<sup>-2</sup> ppb<sup>-1</sup> (parts per billion) and, assuming a 3,200 year lifetime, a global  
79 warming potential of 9,540 on a 100-year timescale (GWP<sub>100</sub>) (Myhre and Shindell et al., 2013; Engel and Rigby et  
80 al., 2018). Due to the long lifetime and high radiative efficiency, emissions of *c*-C<sub>4</sub>F<sub>8</sub> (and other perfluorinated  
81 compounds) essentially permanently alter the radiative budget of Earth (Victor and MacDonald, 1999).

82 Lovelock (1971) predicted the accumulation of *c*-C<sub>4</sub>F<sub>8</sub> in the global atmosphere, but to the best of our knowledge, the  
83 earliest atmospheric measurements of *c*-C<sub>4</sub>F<sub>8</sub> were presented in Sturges et al. (1995) and in the Ph.D. theses of  
84 Travnicek (1998) and Oram (1999, discussed further below). Sturges et al. (2000) determined from one vertical  
85 balloon-borne profile in 1994 that *c*-C<sub>4</sub>F<sub>8</sub> mole fractions declined from ~1.1 ppt (parts per trillion) in the lower  
86 atmosphere of the Northern Hemisphere (NH) to ~0.6 ppt in the stratosphere, while Harnisch (1999) reported that  
87 Sturges et al. (1995) had found 0.4 ppt in the troposphere decreasing to ~0.1 ppt at 25 km in 1994, suggesting a  
88 revised calibration scale. Harnisch et al. (1998; 1999) estimated from this atmospheric gradient global emissions of  
89 1–2 Gg yr<sup>-1</sup> (kt yr<sup>-1</sup>, 1 t = 0.001 Gg). Travnicek (1998) reported ~0.2 ppt in 1977 and ~0.7 ppt in 1997 in the NH  
90 troposphere, from which Harnisch (2000) estimated average global emissions of 0.7 Gg yr<sup>-1</sup>. Despite differences in  
91 early measurements and emissions estimates, perhaps due to different calibration scales and analytical methods,  
92 these studies were consistent with the accumulation of *c*-C<sub>4</sub>F<sub>8</sub> in the global atmosphere.

93 Harnisch (1999, 2000) stated that *c*-C<sub>4</sub>F<sub>8</sub> had limited economic relevance, with some use for plasma etching in the  
94 semiconductor industry, that *c*-C<sub>4</sub>F<sub>8</sub> can be formed via dimerization of tetrafluoroethylene (TFE), and that thermal  
95 decomposition or combustion of polytetrafluoroethylene (PTFE) and other fluoropolymers (Morisaki, 1978) (during  
96 waste disposal) possibly led to the accumulation of atmospheric *c*-C<sub>4</sub>F<sub>8</sub>.

97 Today we have stronger evidence for *c*-C<sub>4</sub>F<sub>8</sub> emissions from the semiconductor and microelectronics industry as it  
98 has been increasingly used since the 1990s for dry etching, chemical vapor deposition chamber cleaning and as  
99 deposition gas (Bosch process). Compared to other fluorinated gases used for these processes, more selective  
100 etching, cost reduction in plasma cleaning, easier abatement and hence potentially lower contribution to global  
101 warming have been cited as advantages of *c*-C<sub>4</sub>F<sub>8</sub> (e.g. Sasaki et al., 1998; Christophorou and Olthoff, 2001; Raju et  
102 al., 2003; Kokkoris et al., 2008; and references therein). However, due to efficient abatement with modern emission  
103 controls (up to 90 %), today's *c*-C<sub>4</sub>F<sub>8</sub> emissions from this industry could also be small (Zhihong et al., 2001).

104 Today we also have further evidence that the thermal decomposition of PTFE and other fluoropolymers can lead to  
105 the formation of *c*-C<sub>4</sub>F<sub>8</sub>, TFE and hexafluoropropylene (HFP) (van der Walt et al., 2008; Bezuidenhoudt et al., 2017);  
106 the resultant *c*-C<sub>4</sub>F<sub>8</sub> could therefore be emitted to the atmosphere.

107 One potentially major source of *c*-C<sub>4</sub>F<sub>8</sub> that seems to have received too little attention is the production of TFE and  
108 HFP monomers, the building blocks for PTFE, fluorinated ethylene propylene (FEP, TFE/HFP copolymer) and other  
109 fluoropolymers, which involves pyrolysis of hydrochlorofluorocarbon 22 (HCFC-22, CHClF<sub>2</sub>) as *c*-C<sub>4</sub>F<sub>8</sub>, the dimer  
110 of TFE, is a by-product/intermediate of this process (Chinoy and Sunavala, 1987; Broyer et al., 1988; Gangal and  
111 Brothers, 2015). This reaction can be steered towards HFP or *c*-C<sub>4</sub>F<sub>8</sub> by controlling the dimerization of TFE to *c*-  
112 C<sub>4</sub>F<sub>8</sub> and the co-pyrolysis of *c*-C<sub>4</sub>F<sub>8</sub> with TFE to HFP (Jianming, 2006). *c*-C<sub>4</sub>F<sub>8</sub> could therefore be emitted during  
113 TFE/HFP/PTFE/FEP production if it is not abated or recovered, e.g. for use in the semiconductor industry or for  
114 pyrolysis with TFE to HFP at a later stage, perhaps at a different facility.

115 Several other, perhaps minor, emissive uses of *c*-C<sub>4</sub>F<sub>8</sub> are also known (see Lewis, 1989; Chung and Bai, 2000;  
116 Harnisch, 2000; Christophorou and Olthoff, 2001; Kim et al., 2002; Liu et al., 2008; and reference therein), e.g. in  
117 foamed/sprayed foods, as a food packaging gas, in retinal detachment surgery, for contrast-enhanced ultrasound  
118 imaging, in radar systems, as a specialty refrigerant (e.g. in submarines where R-405A (43 % *c*-C<sub>4</sub>F<sub>8</sub>) can replace  
119 pure HCFC-22 and the chlorofluorocarbon CFC-12, CCl<sub>2</sub>F<sub>2</sub>), as an electrically insulating dielectric gas (e.g. in  
120 mixtures with sulfur hexafluoride, SF<sub>6</sub>), as a medium for polymerization reactions, in fire extinguishers, and perhaps  
121 as a geohydrological tracer (Kass, 1998). Several chemical reactions in which *c*-C<sub>4</sub>F<sub>8</sub> is used to introduce -CF<sub>3</sub>  
122 groups into organic molecules are known (chemfinder.cas.org, accessed 2019/06/19) as well as reactions leading to  
123 desirable products such as HFO-1234yf, a fourth generation refrigerant used in newer mobile air conditions (MACs,  
124 see Supplement) or HFP, but also various other compounds. Production of *c*-C<sub>4</sub>F<sub>8</sub> for these uses, via the pyrolysis of  
125 HCFC-22 or perhaps from 1,2-dichlorotetrafluoroethane (CFC-114) (Siegemund et al., 2016), may cause emissions  
126 as well. While the major atmospheric PFC, tetrafluoromethane (CF<sub>4</sub>) as well as the minor PFCs hexafluoroethane  
127 (C<sub>2</sub>F<sub>6</sub>) and octafluoropropane (C<sub>3</sub>F<sub>8</sub>) are released during primary aluminum production (Holliday and Henry, 1959;  
128 Tabereaux, 1994; Fraser et al., 2013), no evidence for *c*-C<sub>4</sub>F<sub>8</sub> emissions has been presented so far. Cai et al. (2018)  
129 presented evidence for negligible emissions of *c*-C<sub>4</sub>F<sub>8</sub> from the similar electrolytic production of rare earth elements  
130 in China. There are no known natural sources of *c*-C<sub>4</sub>F<sub>8</sub>. In summary, there may be multiple *c*-C<sub>4</sub>F<sub>8</sub> emission sources,  
131 but the extent and time evolutions of these various potential emission sources are unclear.

132 Saito et al. (2010) reported the first continuous, approximately four year long, in situ measurement record of *c*-C<sub>4</sub>F<sub>8</sub>  
133 at two stations in the NH, with mean baseline 2006–2009 mole fractions of ~1.22 ppt at Cape Oshiishi (43.1° N,  
134 145.3° E) and ~1.33 ppt at Hateruma Island (24.1° N, 123.8° E) (NIES calibration scale). Saito et al. (2010)  
135 determined increase rates of 0.01–0.02 ppt yr<sup>-1</sup> and global emissions of 0.6 ± 0.2 Gg yr<sup>-1</sup>.

136 Oram et al. (2012) published the first multi-decade long atmospheric record of *c*-C<sub>4</sub>F<sub>8</sub> in the Southern Hemisphere  
137 (SH). They combined previous measurements of sub-samples of the Cape Grim Air Archive (CGAA) for the SH  
138 with air dates prior to 1994 (from Oram, 1999, converted to a new, 19.6 % lower calibration scale with an estimated  
139 uncertainty of ≤7 %) with newer measurements of CGAA sub-samples with air dates after 1994 and a change of  
140 analytical method after 2006. They found an increase of *c*-C<sub>4</sub>F<sub>8</sub> at Cape Grim from 0.35 ppt in 1978 to ~0.8 ppt in  
141 1995 and 1.2 ppt in 2010, with a current increase rate of ~0.03 ppt yr<sup>-1</sup>. They reported that global *c*-C<sub>4</sub>F<sub>8</sub> emissions  
142 increased from ~0.9 Gg yr<sup>-1</sup> in the early 1980s to ~1.7 Gg yr<sup>-1</sup> in 1986 before declining to a minimum of ~0.4 Gg yr<sup>-1</sup>  
143 in 1993, after which they increased to ~1.1 Gg yr<sup>-1</sup> in 2006 and 2007 and may have stabilized. Oram et al. (2012)

144 noted that the global emissions determined by Saito et al. (2010) were lower than their estimate and suggested that  
145 the underlying atmospheric rise rate measured by Saito et al. may be too small.

146 In summary, calibration differences between previous studies are significant, no multi-decadal *c*-C<sub>4</sub>F<sub>8</sub> record for the  
147 NH has been published, and global emissions have not been reassessed since Oram et al. (2012). Therefore our  
148 primary goals have been to develop an independent gravimetric *c*-C<sub>4</sub>F<sub>8</sub> calibration scale and to characterize the  
149 abundances of *c*-C<sub>4</sub>F<sub>8</sub> with high precisions in both hemispheres in order to determine updated historic and recent  
150 global emissions. We present measurements of *c*-C<sub>4</sub>F<sub>8</sub> with precisions of ~1–2 % on the SIO-14 calibration scale (~2  
151 % accuracy) developed by the Scripps Institution of Oceanography (SIO) using instrumentation and calibration  
152 methods of the Advanced Global Atmospheric Gases Experiment (AGAGE) program (Prinn et al., 2018). We  
153 discuss historic atmospheric mole fractions of *c*-C<sub>4</sub>F<sub>8</sub> based on measurements of the CGAA for the extra-tropical SH,  
154 archived air samples from various sources for the extra-tropical NH, continuous atmospheric measurements in both  
155 hemispheres at multiple remote AGAGE stations since mid-2010, combined with measurements of air extracted from  
156 firn from both hemispheres. Using our measurements and inverse modelling methods, we infer global *c*-C<sub>4</sub>F<sub>8</sub>  
157 emissions since the beginning of the 20<sup>th</sup> century until 2017. To improve our understanding of prominent *c*-C<sub>4</sub>F<sub>8</sub>  
158 sources and source regions, we investigate regional *c*-C<sub>4</sub>F<sub>8</sub> emission strengths as observed by the global AGAGE  
159 network in eastern Asia, Europe, parts of Australia and Russia and by an aircraft campaign over India. We also  
160 summarize and discuss available inventory based “bottom-up” emissions and compare them to the emissions we  
161 determined with our atmospheric measurement based “top-down” approach.

## 162 **2 Experimental methods**

### 163 **2.1 Instrumentation, data availability, and calibration**

164 *c*-C<sub>4</sub>F<sub>8</sub> and ~40 other halogenated compounds were measured by AGAGE in 2 L air samples with the “Medusa”  
165 cryogenic pre-concentration system with gas chromatograph (GC, Agilent 6890) and quadrupole mass selective  
166 detector (MSD) (Miller et al., 2008; Prinn et al., 2018). Data from twelve in situ measurements sites and fourteen  
167 Medusa instruments were used. At Monte Cimone, Italy, *c*-C<sub>4</sub>F<sub>8</sub> was measured with a commercial Adsorption-  
168 Desorption System with gas chromatograph and mass spectrometer (ADS-GC/MS) (Maione et al., 2013). Table 1  
169 shows the availability of in situ, archived air (Sect. 2.2), firn air (Sect. 2.3) and aircraft air sample (Sect. 2.4)  
170 measurements with information for each site. For all measurements, each sample was alternated with a reference gas  
171 (Prinn et al., 2000; Miller et al., 2008), resulting in up to 12 fully calibrated samples per day (Medusa and ADS-  
172 GC/MS). The reference gases at each site were calibrated relative to parent standards at SIO.

173 *c*-C<sub>4</sub>F<sub>8</sub> measurements are reported on the SIO-14 calibration scale as ppt dry-air mole fractions. The calibration scale  
174 is based on four gravimetric halocarbon/nitrous oxide (N<sub>2</sub>O) mixtures via a stepwise dilution technique with large  
175 dilution factors for each step (10<sup>3</sup> to 10<sup>5</sup>) (Prinn et al., 2000; 2001). High purity *c*-C<sub>4</sub>F<sub>8</sub> (99.999 %, Matheson Trigas)  
176 and N<sub>2</sub>O (99.9997 %, Scott Specialty Gases) were further purified by repeated cycles of freezing (-196° C), vacuum  
177 removal of non-condensable gases, and thawing. Artificial air (Ultra Zero Grade, Airgas) was further purified via an  
178 absorbent trap filled with glass beads, Molecular Sieve (MS) 13X, charcoal, MS 5Å, and Carboxen 1000 at -80° C

179 (ethanol/dry ice). Zero air was measured to verify insignificant *c*-C<sub>4</sub>F<sub>8</sub> and other halocarbon blank levels before  
180 being spiked with the *c*-C<sub>4</sub>F<sub>8</sub>/N<sub>2</sub>O mixtures. The resulting mixtures of *c*-C<sub>4</sub>F<sub>8</sub> in artificial air have prepared values of  
181 ~1.3 ppt and the relative standard deviation of the calibration scale is 0.23 %. We estimate the uncertainties of the  
182 calibration scale propagation from SIO to the sites to be ~0.6 % and the calibration scale uncertainty to be ~2 % (see  
183 Prinn et al., 2000, 2001, 2018).

184 The primary calibration instrument for the AGAGE network at SIO (La Jolla, California), Medusa 1, and all field  
185 instruments used a Porabond Q (25 m, 0.32 mm I.D., 5 μm film thickness, Varian) chromatographic main column  
186 and, initially Agilent 5973, later 5975 series MSDs. The original Medusa design is described by Miller et al. (2008);  
187 subsequently all Medusas were converted or newly built to measure nitrogen trifluoride (NF<sub>3</sub>) (Arnold et al., 2012),  
188 but this did not affect the *c*-C<sub>4</sub>F<sub>8</sub> measurements methodology or the results. While 5975 MSDs are beneficial for  
189 samples and compounds with very low mole fractions, precisions for *c*-C<sub>4</sub>F<sub>8</sub> measurements of archived air samples  
190 (3–7 replicates, see next section) were similar, i.e. better than ~0.01 ppt. Daily reference gas measurement precisions  
191 slightly improved from ~0.02 ppt (~1.5–2 %) to ~0.01 ppt (~1–1.5 %) with the 5975 MSDs. Detection limits (3 times  
192 baseline noise) for 2 L air samples were ~0.01–0.03 ppt for both types of MSDs.

193 In addition to calibrations, Medusa 1 was also used to measure in situ local ambient air and several archived air  
194 samples (see Sect. 2.2). However, analysis of most archived air samples at SIO occurred on a second instrument,  
195 Medusa 7, as it was equipped with a more sensitive 5975 MSD at that time. For these measurements, we temporarily  
196 converted Medusa 7 to use a GasPro GSC (60 m, 0.32 mm I.D., Agilent) main column as it promised better  
197 separation performance for several higher PFCs (Ivy et al., 2012) measured along with *c*-C<sub>4</sub>F<sub>8</sub>. Similarly, Medusa 9,  
198 the instrument used to measure most CGAA samples at the Commonwealth Scientific and Industrial Research  
199 Organisation (CSIRO, Aspendale) and ambient air after October 2010, had been converted to use a GasPro column.  
200 On both types of main columns, *c*-C<sub>4</sub>F<sub>8</sub> was measured on mass over charge ratios (*m/z*) of 131 (C<sub>3</sub>F<sub>5</sub><sup>+</sup>) and 100  
201 (C<sub>2</sub>F<sub>4</sub><sup>+</sup>) and reported by height using carefully chosen integration parameters as perfluorobutane (C<sub>4</sub>F<sub>10</sub>) shares both  
202 *m/z* and elutes on the tail of *c*-C<sub>4</sub>F<sub>8</sub>. The *m/z* ratios remained the same despite the very different separation principles  
203 of these two main columns. Measurements of archived air samples on Medusa 7 with both main columns agreed  
204 within less than 0.01 ppt (ratio of 1.0016, R<sup>2</sup> = 1.0000, n = 4, 0.237–1.11 ppt). In situ *c*-C<sub>4</sub>F<sub>8</sub> measurements at SIO  
205 with Medusa 1 (Porabond Q) and 7 (with the GasPro column) continued to agree within typical precisions. We also  
206 compared archived air measurements on Medusa 1 and 7, both before and while Medusa 7 used the GasPro column,  
207 and results agree within precisions of 0.02 ppt or better (Medusa 1 vs. Medusa 7, both Porabond Q, ratio of 1.0001,  
208 R<sup>2</sup> = 0.9987, n = 95, 0.237–1.616 ppt, Medusa 1, Porabond Q vs. Medusa 7, GasPro, ratio of 1.0018, R<sup>2</sup> = 0.9979, n  
209 = 39, 0.239–1.515 ppt). These tests show that the different main columns did not cause any bias.

210 The analytical systems showed no significant *c*-C<sub>4</sub>F<sub>8</sub> blanks. The linearity of Medusa 7 (SIO) and 9 (CSIRO) used to  
211 measure archived air samples was assessed with a series of diluted air samples (parent tank at 1.252 ppt, dilutions  
212 from 100 % to 6.25 %, Ivy et al., 2012) and a series of different volumes of a working standard (parent tank at 1.60  
213 ppt, sample volumes from 200 % to 5 % of usual 2 L volume). A small deviation from linearity was observed for the  
214 most diluted samples and the smallest volumes, probably due to a memory or blank of ~0.014 ppt on Medusa 9, for  
215 which a correction was applied. Medusa 7 showed an effect of ~0.008 ppt, but as this was just below the detection  
216 limits and within the typical precisions, we chose not to correct for this.

217 **2.2 Archived air samples of the extra-tropical Southern Hemisphere (SH, Cape Grim Air Archive, CGAA)**  
218 **and extra-tropical Northern Hemisphere (NH)**

219 To reconstruct the atmospheric history of *c*-C<sub>4</sub>F<sub>8</sub> in the extra-tropical SH, 41 unique CGAA samples (collected  
220 1978–2009, Langenfelds et al., 2014) were measured at CSIRO in 2011 (Ivy et al., 2012). In addition, 8 subsamples  
221 of CGAA parent tanks and four additional SH samples were measured at SIO to demonstrate that measurements at  
222 CSIRO and SIO agree (for details see the Supplement). Based on an iterative filtering process designed to reject  
223 outliers greater than 2σ deviations from curve fits through the results for all 60 SH samples (41 at CSIRO and 19 at  
224 SIO) and pollution filtered monthly mean measurements (O'Doherty et al., 2001; Cunnold et al., 2002) at the extra-  
225 tropical stations CGO and ASA (Australia), 13 SH samples were rejected as outliers, leaving 47 SH samples (78 %).  
226 To reconstruct the atmospheric history in the extra-tropical NH, 126 unique air samples mostly filled at SIO and  
227 THD (1973–2016) were measured at SIO. Additionally, 3 NH samples (filled in 1980 and 1999) were measured at  
228 CSIRO to demonstrate that measurements at CSIRO and SIO agree (for details see the Supplement). Most of the NH  
229 samples had been filled during baseline conditions for various purposes using modified diving compressors (RIX  
230 Industries, US, SA-3 and SA-6, Weiss and Keeling laboratories) and did not show any artefacts for many gases (e.g.  
231 Mühle et al., 2010; O'Doherty et al., 2014; Vollmer et al., 2016). For *c*-C<sub>4</sub>F<sub>8</sub>, however, comparisons with concurrent  
232 in situ measurements at MHD, THD, SIO and JFJ revealed artefacts for most of these samples and the iterative  
233 filtering process only retained *c*-C<sub>4</sub>F<sub>8</sub> data for eleven NH samples. In contrast, CGAA tanks were filled with a  
234 cryogenic method which did not produce any bias. Due to the sparse NH data and poor data quality before in situ  
235 measurements started in the NH, the fits used for the iterative filtering process of NH data had to be guided by the  
236 final SH fit shifted by 1.5 years to allow for the delay of *c*-C<sub>4</sub>F<sub>8</sub> accumulation between the SH and NH due to inter-  
237 hemispheric transport (Mühle et al., 2010; Vollmer et al., 2016). Without this guidance, initial NH fits were  
238 dominated by high outliers, resulting in bad fits. It should be pointed out that most of the filtered NH tanks were  
239 filled in 2003 and later, typically many tanks on one or two days in a given year, which would add little information  
240 to the reconstruction given the onset of in situ data at multiple stations in 2011 and the high quality of the CGAA  
241 data used to guide the filtering. Fig. 1 shows the filtered data and the final suggested fits and 95% confidence bands.

242 **2.3 Air extracted from firn**

243 To augment the data set of in situ and archived air measurements, we measured *c*-C<sub>4</sub>F<sub>8</sub> in samples from a subset of  
244 the firn sites described in Trudinger et al. (2016), namely NEEM08 in the NH and DSSW20K and SPO01 in the SH,  
245 plus one new site in the NH, Summit13, Greenland. We used the CSIRO firn model (Trudinger et al., 1997;  
246 Trudinger et al., 2013) to characterize the age of the air in these samples (detailed in Sect. 4.1). Here, we give a brief  
247 description of the firn sites. For a full description of the calibration of the CSIRO firn model for NEEM08,  
248 DSSW20K, and SPO01 see Trudinger et al. (2013), and for Summit13 see Fig. S1.

249 NEEM08: Firn air was extracted from the EU borehole in July 2008 in northern Greenland, drilled near the North  
250 Greenland Eemian Ice Drilling Project (NEEM) deep ice core drilling site (77.45° N, 51.06° W) (Buizert et al.,  
251 2012). This site has a moderate snow accumulation rate of 199 kg m<sup>-2</sup> yr<sup>-1</sup>.

252 Summit13: Firn air was collected in May 2013 at Summit, Greenland from a borehole (72.66° N, 38.58° W) drilled  
253 10 km NNW of Summit Station, Greenland. The US Firn Air system (Battle et al., 1996) was used to extract the air

254 from 19 depth levels in the firn from the surface to just above 80.06 m (below this depth firn air can no longer be  
255 collected as the open channels in firn have closed off and formed discrete bubbles embedded in ice). The 3 in  
256 borehole was drilled with the Eclipse Ice Drill (IDDO) and new rubber bladders (1/8 in thick) were fabricated  
257 (Greene Rubber Co., Woburn, MA) for use in this campaign. 2.5 L glass flasks were filled at all depths for high  
258 resolution measurements of gases performed by the National Oceanic and Atmospheric Administration (NOAA)  
259 ( $\text{CO}_2$ ,  $\text{CH}_4$ ,  $\text{CO}$ ,  $\text{N}_2\text{O}$ ,  $\text{SF}_6$ ,  $\text{H}_2$ ). Larger volume samples from pre-selected depth levels were filled in 35 L electro-  
260 polished SS tanks using a KNF Neuberger pump (with neoprene diaphragms). These samples were measured at SIO  
261 for  $c\text{-C}_4\text{F}_8$  and other trace gases (including  $\text{CH}_4$ ,  $\text{N}_2\text{O}$ , CFCs, HFCs, HCFCs, and  $\text{SF}_6$ ). For quality control purposes,  
262 the sample line was measured on site for  $\text{CO}_2$  and  $\text{CH}_4$  by cavity ring-down spectroscopy (CRDS, Los Gatos  
263 Research,  $\mu\text{-GGA}$ ) and  $[\text{CO}]$  by a reducing compound photometer (Peak Labs, RCP1) prior to filling the flasks.  
264 Summit has a moderate snow accumulation rate of  $211 \text{ kg m}^{-2} \text{ yr}^{-1}$ . CSIRO firn model calculations for Summit use  
265 the density profile from Adolph and Albert (2014) and mean annual temperature and pressure of 241.75 K and 665  
266 mbar. The diffusivity profile and related parameters were calibrated using the measurements described above of  $\text{CO}_2$ ,  
267  $\text{CH}_4$ ,  $\text{N}_2\text{O}$ ,  $\text{SF}_6$ , CFC-11, CFC-12, CFC-113,  $\text{CH}_3\text{CCl}_3$ , HFC-134a, HCFC-141b, and HCFC-142b. Firn model results  
268 for these tracers are shown in Fig. S1.

269 DSSW20K: Firn air was collected in January 1998 in Eastern Antarctica ( $66.73^\circ \text{ S}$ ,  $112.83^\circ \text{ E}$ ) from a borehole  
270 drilled 20 km west of the deep Dome Summit South (DSS) drill site near the summit of Law Dome (Smith et al.,  
271 2000; Sturrock et al., 2002; Trudinger et al., 2002). This site has a short firn column and a moderate snow  
272 accumulation rate of  $150 \text{ kg m}^{-2} \text{ yr}^{-1}$ .

273 SPO01: We only measured one sample collected in 2001 from 120 m from a borehole at the South Pole, Antarctica  
274 ( $90^\circ \text{ S}$ ,  $119^\circ \text{ W}$ ) (Aydin et al., 2004; Sowers et al., 2005). This site has a deep firn column and a low snow  
275 accumulation rate of  $75 \text{ kg m}^{-2} \text{ yr}^{-1}$ , resulting in old firn air.

276 Firn air extracted from the DSSW20K, NEEM08, and SPO01 sites was measured at CSIRO in 2012 (Medusa 9),  
277 while Summit13 firn air was measured at SIO (Medusa 7), see Table 1.  $c\text{-C}_4\text{F}_8$  firn measurement data are included in  
278 the data file listed in the Supplement. Other gases such as  $\text{CH}_4$  and  $\text{N}_2\text{O}$  were measured as well.

#### 279 **2.4 Air samples collected over India and the Indian Ocean**

280 Air samples were collected on-board the UK FAAM (Facility for Airborne Atmospheric Measurements) BAe-146  
281 aircraft during eleven flights conducted from June 12, 2016 to July 9, 2016 ( $9\text{--}28^\circ \text{ N}$ ,  $72\text{--}86^\circ \text{ E}$ ) into 3 L pre-  
282 evacuated electropolished SS flasks (SilcoCan, Restek) sealed with metal bellow valves (SS-BNVVCR-4,  
283 Swagelok). During the time it took to compress the air samples to 41 psig (30–60 s, depending on altitude) using a  
284 metal bellows pump (PWSC 28823-7, Senior Aerospace, USA), the aircraft travelled  $\sim 7$  km. Nine flights occurred  
285 over Northern India and two over Southern India and the Indian Ocean. In total, 176 flask samples were collected,  
286 with the majority ( $>90\%$ ) of these samples filled below 1.5 km altitude. The size of the subsamples analyzed with  
287 the Medusa 21 at University of Bristol was reduced to 1.75 L (from 2 L) and the sampling rate to  $50 \text{ ml min}^{-1}$  (from  
288  $100 \text{ ml min}^{-1}$ ) to allow for triplicate analyses of each flask and to accommodate for the lower flask pressure.  $c\text{-C}_4\text{F}_8$   
289 measurements are reported on the SIO-14 calibration scale. Detection limits, blanks, and precisions were similar to  
290 those stated above. For further details, see Say et al. (2019).



### 291 **3 Bottom-up emission inventories (UNFCCC, EDGAR, NIRs, WSC)**

292 Emissions of compounds, such as *c*-C<sub>4</sub>F<sub>8</sub>, into the atmosphere are often estimated by so called “bottom-up” methods,  
293 which are based on information such as purchased, produced or imported amounts, industrial activities referred to as  
294 activity data and estimated emissions factors for each emissive process. Developed countries report annual emissions  
295 of GHG, including *c*-C<sub>4</sub>F<sub>8</sub>, to the UNFCCC using such bottom-up methods. However, these data are inherently not  
296 representative of total global emissions since developing countries do not have the same comprehensive UNFCCC  
297 reporting requirements, including countries such as South Korea, China, and Taiwan with sizable electronics and  
298 PTFE manufacturing capacities and thus with potentially significant *c*-C<sub>4</sub>F<sub>8</sub> emissions. An additional complication is  
299 that several countries report unspecified mixes of PFCs or of PFCs and HFCs and other fluorinated compounds,  
300 making it difficult or impossible to estimate emissions of individual compounds, such as *c*-C<sub>4</sub>F<sub>8</sub>. In the Supplement,  
301 we gather available inventory information from submissions to UNFCCC, National Inventory Reports (NIRs), the  
302 Emissions Database for Global Atmospheric Research (EDGAR), the World Semiconductor Council (WSC), and the  
303 US Environmental Protection Agency (EPA) in an effort to estimate contributions from unspecified mixes and  
304 countries not reporting to UNFCCC to compile a meaningful bottom-up inventory. Globally these add up to 10–30 t  
305 yr<sup>-1</sup> (0.01–0.03 Gg yr<sup>-1</sup>) from 1990 to 1999, 30–40 t yr<sup>-1</sup> (0.03–0.04 Gg yr<sup>-1</sup>) from 2000 to 2010, and 100–116 t yr<sup>-1</sup>  
306 (~0.1 Gg yr<sup>-1</sup>) from 2011 to 2014 (with a substantial fraction due to the U.S. emissions from fluorocarbon production  
307 reported by US EPA). As has been found by Saito et al. (2010) and Oram et al. (2012), we show in Sect. 5.2 and 5.3  
308 that measurement based (“top-down”) global and most regional emissions are significantly larger than the compiled  
309 bottom-up *c*-C<sub>4</sub>F<sub>8</sub> emissions inventory information (see Fig. 5), analogous to what has been found for other PFCs  
310 (Mühle et al., 2010), reflecting the shortcomings of current emission reporting requirements and inventories.

### 311 **4 Modelling studies**

#### 312 **4.1 CSIRO firm model**

313 The CSIRO firm model and its use in global inversion frameworks has been described in detail (Trudinger et al.,  
314 2013; Trudinger et al., 2016; Vollmer et al., 2016; Vollmer et al., 2018; Vollmer et al., 2019). Air samples taken far  
315 away from pollution sources represent the background atmospheric trace gas composition at that time. Once air  
316 enters the firm, vertical diffusion and other physical processes in the firm lead to mixing of air of different ages.  
317 Therefore, air extracted from firm must be described with an age distribution. We used the CSIRO firm model to  
318 describe the relationship between trace gas mole fractions measured in each extracted air sample from a given depth  
319 and the corresponding age distribution of high-latitude atmospheric mole fractions. The diffusion coefficient of *c*-  
320 C<sub>4</sub>F<sub>8</sub> relative to that of CO<sub>2</sub> in air at 253 K used here was 0.47 with an estimated uncertainty of ~10 %. This value  
321 was determined using Equation 4 from Fuller et al. (1966) with Le Bas volume increments (e.g. Table 1.3.1, Mackay  
322 et al. (2006) and a multiplier for the Le Bas increments of 0.97 (which minimizes the difference of calculated relative  
323 diffusion coefficients of a number of compounds from values measured by Matsunaga et al. (1993, 2002, 2005)).

324 Figure 2 shows the measured depth profile of  $c\text{-C}_4\text{F}_8$  (ppt) in air extracted from polar firn sites in the NH (Greenland)  
325 and the SH (Antarctica), for site details see Table 1. All samples showed  $c\text{-C}_4\text{F}_8$  mole fractions above the detection  
326 limit. The firn reconstructed depth profiles are discussed in Sect. 4.3.1.

## 327 4.2 AGAGE 12-box model of the global atmosphere

328 The AGAGE 12-box two-dimensional model (Cunnold et al., 1983; Cunnold et al., 1997; Rigby et al., 2013)  
329 describes the transport and loss of trace gases in the global atmosphere. The model divides the atmosphere into four  
330 latitudinal bands at  $0^\circ$  and  $30^\circ$  S/ $^\circ$  N and three altitude bands at 500 hPa and 200 hPa and calculates the mole  
331 fractions in each box. The AGAGE background sites (MHD, THD, RPB, SMO and CGO, see Table 1) were  
332 historically chosen to represent the trace gas mole fractions in the four lower (tropospheric) model “boxes”. Model  
333 transport parameters were varied seasonally, but repeated annually. Given the very long atmospheric lifetime of  $c\text{-}$   
334  $\text{C}_4\text{F}_8$  compared to the study period, the lifetime of  $c\text{-C}_4\text{F}_8$  was assumed to be infinite in the model.

## 335 4.3 Global inversion methods

336 We used the AGAGE 12-box model in two different Bayesian inversions, denoted as the “CSIRO” and “Bristol”  
337 inversions, to estimate historic  $c\text{-C}_4\text{F}_8$  emissions from our observations and to reconstruct historic abundances. Both  
338 inversions used in situ and archive data and the CSIRO inversion additionally used firn data. The observations need  
339 to be representative of clean background air at each sampling location. For in situ data, the AGAGE statistical  
340 method was used to remove pollution events and to calculate pollution-free monthly mean background air mole  
341 fractions for each AGAGE station (O'Doherty et al., 2001; Cunnold et al., 2002). As explained in Sect. 2.2, an  
342 iterative filtering algorithm starting out with all the archived air data and the pollution-free monthly means was then  
343 used to reject outliers for the extra-tropical SH and NH, mostly from the NH archive data. Due to the remoteness of  
344 the firn sample sites, we assumed background conditions without any filtering.

### 345 4.3.1 CSIRO inversion

346 The CSIRO inversion was developed to infer annual emissions at the global scale from firn, ice core and atmospheric  
347 measurements (Sturrock et al., 2002; Trudinger et al., 2002; Trudinger et al., 2016). Green’s functions from the  
348 CSIRO firn model were used to relate the measured air in the firn samples to air in the atmosphere in the past, and  
349 Green’s functions from the AGAGE 12-box model were used to relate global emissions with a specified latitudinal  
350 distribution to mole fraction in the extra-tropical SH and NH. The inversion included constraints to avoid negative  
351 mole fractions, negative emissions and unrealistic changes in emissions; these constraints were required due to the  
352 characteristics of inverting firn data and sparse archive data. The uncertainties in reconstructed mole fractions and  
353 inferred emissions were calculated using a bootstrap method that included the uncertainty in firn measurements,  
354 annual mean mole fraction (this uncertainty is temporally-correlated, see Supplement in Vollmer et al., 2019),  
355 calibration scale ( $\pm 2\%$ ), and the firn model through the use of an ensemble of Green’s functions corresponding to  
356 different firn model parameters including relative diffusivity (Trudinger et al., 2013; Trudinger et al., 2016; Vollmer  
357 et al., 2016).

358 Figure 3 shows the data that were used in the CSIRO inversion: annual values based on 10-year smoothing spline fits  
359 (i.e. 50 % attenuation at periods of 10 years) to monthly means of pollution-free in situ measurements at the AGAGE  
360 background sites CGO (SH) and MHD (NH), annual values based on 10-year smoothing spline fits to measurements  
361 of the CGAA and archived NH air samples, and air extracted from polar firn in both hemispheres. Annual means  
362 from the spline were only used in the inversion when there were pollution-free archive or in situ measurements  
363 around that time. Figure 3 also shows the final reconstructed abundances for the extra-tropical SH (solid black line)  
364 and NH (dashed black line) based on the optimized emissions. The measured mole fractions in firn air are plotted  
365 against their effective atmospheric ages if that age is after 1965, where the effective ages are calculated using the  
366 reconstructed history of atmospheric mole fractions determined by the CSIRO inversion (Trudinger et al., 2002).  
367 Before 1965, the growth rate in the atmosphere was small and uncertain; this makes it difficult to determine effective  
368 ages, so the earlier firn measurements are plotted against their mean ages (see also Fig. S7). Firn depth profiles for  
369 each firn site corresponding to the CSIRO inversion results are shown in Fig. 2 (solid lines) and they typically agree  
370 with the measurements within precisions ( $1\sigma$ , shown as error bars).

371 Overall, the abundances reconstructed with the CSIRO inversion agree very well with the measurement data (see  
372 also Fig. S2). In Fig. S3, we show the effect of excluding different sites from the inversion on reconstructed  
373 emissions and mixing ratios and the sensitivity of the inversion to the relative diffusion coefficient of  $c\text{-C}_4\text{F}_8$ .

374 It should be pointed out that the deepest NEEM08 firn air sample for the NH showed slightly lower mole fractions  
375 (0.0085 ppt) than the deepest DSSW20K samples for the SH (0.021 ppt and 0.0185 ppt), although the mean ages are  
376 similar (1930s). The same applies to the second deepest NEEM08 (0.0105 ppt) and DSSW20K (0.018 ppt) samples  
377 (1940s), which is unexpected for a long-lived anthropogenic compound predominantly emitted in the NH. While the  
378 differences seem significant within the nominal precisions (0–0.0014 ppt) achieved for these firn samples measured  
379 only 1–2 times, they are not significant within typical precisions achieved for archive samples ( $\sim 0.01\text{--}0.02$  ppt)  
380 which are typically measured 3 or more times and these data are just at or below the typical detection limits of 0.01–  
381 0.03 ppt. Based on the order in which the firn samples were measured and the absence of detectable blanks, it seems  
382 unlikely that a small blank, memory, calibration, or measurement problem could have caused this small discrepancy.  
383 The early part of the reconstructed record, with near-zero mole fractions, is also most susceptible to small  
384 uncertainties in the calibrated diffusivity profiles versus depth for all sites used in the firn model, uncertainties in the  
385 firn model structure (e.g. physical properties being invariant of time), or uncertainties in the diffusivity of different  
386 tracers relative to each other. Thus, there are a number of possible reasons for the higher mixing ratio in the SH firn  
387 data at this time, and we do not interpret this as evidence of higher mole fraction in the SH in the 1930s or 1950s.

#### 388 **4.3.2 Bristol inversion**

389 The Bristol inversion was used to estimate annual fluxes of  $c\text{-C}_4\text{F}_8$  using archive and in situ observations only (Rigby  
390 et al., 2011; Rigby et al., 2014; Vollmer et al., 2018). A priori, it was assumed that emissions were similar from year  
391 to year such that the a priori year-to-year emissions growth rate was assumed to be zero with an uncertainty of 200 t  
392  $\text{yr}^{-2}$  ( $0.2 \text{ Gg yr}^{-2}$ ,  $1\sigma$ ), approximately twice the bottom-up estimate in Sect. 3. The derived emissions uncertainties  
393 include contributions from the measurement repeatability, the calibration scale uncertainty, and the model-  
394 measurement representation error (Rigby et al., 2014). Furthermore, because some archive air samples exhibit

395 substantial short-timescale ( $< 1$  year) variations that are unlikely to represent real changes in the background  
396 atmosphere (Fig. 1), the minimum uncertainty was set to the maximum deviation of the archive air samples from the  
397 smooth curve in Fig. 1 (0.03 ppt). Model representation errors were estimated as the variability of the pollution-free  
398 monthly baseline means determined by the AGAGE pollution algorithm (O'Doherty et al., 2001; Cunnold et al.,  
399 2002) from the high-frequency in situ data at each station for each given month. For periods without in situ data, the  
400 representation error was assumed to be equal to the average baseline variability from in situ data in the same  
401 latitudinal band scaled by the measured  $c\text{-C}_4\text{F}_8$  abundance. The calibration scale propagation uncertainty is estimated  
402 based on propagation uncertainties of the  $c\text{-C}_4\text{F}_8$  calibration scale from primary gravimetric standards to secondary  
403 standards within the “R1” relative calibration framework used in AGAGE and on propagation uncertainties from the  
404 R1 framework to the standards used to measure individual samples. Figure 4 shows that there is good agreement  
405 between the archived air samples (Sect. 2.2) and the pollution-free monthly mean in situ data from the AGAGE  
406 background sites (MHD and THD, RPB, SMO, and CGO) used in the Bristol inversion and the reconstructed mole  
407 fractions for the four latitudinal bands which these samples represent (see also Fig. S4).

#### 408 **4.4 Regional model and inversion study using NAME-HB for eastern Asia**

409 To investigate regional emissions in eastern Asia ( $20^\circ\text{ N}$ – $50^\circ\text{ N}$  and  $110^\circ\text{ E}$ – $160^\circ\text{ E}$ ) from our observations we used  
410 an inversion method based on Bayesian inference. We estimated annual mean emissions, assuming that emissions are  
411 constant in both space and magnitude during each calendar year. Here, the inversion used observations from the  
412 Gosan station as this site was operated with relatively few interruptions from October 2010 to the end of 2017, with  
413 best data coverage from 2011 to 2015. These observations were binned into 12 hourly averages. The inversion  
414 method requires an atmospheric transport model to derive the sensitivity of the observations to a surface emissions  
415 field. We used the Lagrangian NAME (Numerical Atmospheric dispersion Modelling Environment) model from the  
416 UK Met Office (Jones et al., 2007), driven by meteorology from the Met Office Unified Model (Walters et al., 2014).  
417 The sensitivity was derived by releasing 20,000 hypothetical air parcels per hour of measurement from Gosan  
418 station, which were transported backwards in time for up to 30 days. The model recorded the time and location that  
419 air parcels interacted with the surface (below 40 m above ground level at a spatial resolution of  $0.352^\circ$  by  $0.234^\circ$ ),  
420 and these data were used to form an aggregated 30-day sensitivity or “footprint” map for each hour of measurement.  
421 In addition, the model recorded the time and location that air parcels left the domain boundaries to provide the  
422 sensitivity to the boundary conditions. The footprint maps, generated over the domain  $5^\circ\text{ S}$ – $74^\circ\text{ N}$  and  $55^\circ\text{ E}$ – $192^\circ\text{ E}$   
423 and up to 19 kilometres, were aggregated into 12 hourly averages.

424 We used a trans-dimensional hierarchical Bayesian method (NAME-HB) with a Metropolis-Hastings Markov chain  
425 Monte Carlo (MCMC) algorithm (Metropolis et al., 1953; Hastings, 1970) to solve the inverse problem. This  
426 allowed spatial emission estimates of  $c\text{-C}_4\text{F}_8$  to be derived, whilst considering the uncertainties in the model,  
427 measurements, and a priori information and, importantly, the uncertainty in these uncertainties. Bayesian methods  
428 require a priori knowledge, here the emissions and boundary conditions. As little information on eastern Asia’s  $c\text{-}$   
429  $\text{C}_4\text{F}_8$  emissions (see Sect. 3) was available, we based our mean a priori emissions on those estimated by Saito et al.  
430 (2010). We spread their emissions for each reported country uniformly over the area of each country, rather than use  
431 population density (as in Saito et al., 2010) as that is not likely a good proxy of  $c\text{-C}_4\text{F}_8$  emissions. We also spread

432 0.11 Gg yr<sup>-1</sup> of emissions over the rest of the domain where the footprint was calculated. The value of 0.11 Gg yr<sup>-1</sup> is  
433 an approximate scaling of the global total emissions based on population in this outer domain, i.e. the remainder of  
434 the domain not defined as eastern Asia. While we do not report emission estimates outside of eastern Asia due to  
435 large posterior uncertainties, they are still estimated in the inversion as they are useful when modelling the emissions  
436 in eastern Asia and their uncertainties that we do report. We assigned a large uncertainty to these a priori emissions  
437 (Table S1), which were governed by a log-normal distribution, so that they were uninformative and the observations  
438 dominated the estimation. We set a priori boundary conditions to be the mean background mole fractions measured  
439 at MHD on each vertical boundary (N, E, W, S) of the NAME domain. Offsets to the boundary conditions on each  
440 boundary were estimated in the inversion on a monthly basis.

441 The hierarchical nature of the inversion method means that hyper-parameters were also incorporated to include  
442 uncertainties in the NAME sensitivities, which are described by a multivariate normal distribution (see Ganesan et  
443 al., 2014). The reversible jump, or trans-dimensional, aspect of the inversion means that the underlying resolution at  
444 which the emissions are estimated is itself explored during inference (Lunt et al., 2016). Table S1 shows the a priori  
445 probability distributions assigned to the emissions and boundary conditions scaling factors, model uncertainty and  
446 the underlying grid. The posterior emissions estimates and their uncertainties were governed by exploring the spaces  
447 of each of these parameters and hyper-parameters. The sensitivity of the emissions generally decreases with distance  
448 from the measurement site, which leads to increased uncertainty in the inversion, both in the spatial distribution of  
449 emissions and their overall magnitude. The further away emissions occur, the more likely the regional inversion  
450 method will allocate these emissions to a general diffuse region, rather than identify individual *c*-C<sub>4</sub>F<sub>8</sub> point sources.

#### 451 **4.5 Regional model and inversion study using InTEM for Western Europe**

452 To investigate regional emissions in Western Europe (36° N–66° N and -14° E–31° E) we used InTEM, an inversion  
453 framework (Arnold et al., 2018) based on the NAME Lagrangian transport model (Jones et al., 2007), together with  
454 observations from MHD, Tacolneston (TAC), Jungfraujoch (JFJ) and Monte Cimone (CMN). A priori estimates  
455 were considered unknown (see Sect. 3 and the Supplement) and therefore set to a uniform distribution of 0.2 Gg yr<sup>-1</sup>  
456 over the whole land area within the inversion domain with an uncertainty of 0–0.62 Gg yr<sup>-1</sup>. Observational  
457 uncertainty was time varying and estimated as the variability of the observations in a 6 hour moving window plus the  
458 measurement repeatability determined from repeat measurements of the on-site calibration standards. Model  
459 uncertainty was estimated every 2 hours as the larger of the median of all pollution events at each station in a year or  
460 16.5 % of the magnitude of the pollution event. A temporal correlation of 12 hours was assumed in the model  
461 uncertainty at each station. An analytical solution was found that minimized the residual between the model and the  
462 observations and the difference between the posterior and the a priori flux estimate, balanced by the uncertainties of  
463 both. The baseline was estimated in the inversion following Arnold et al. (2018). The variable resolution of the  
464 inversion grid was calculated and refined within InTEM based on the magnitude of the footprint and emissions from  
465 each grid box. The inversions were run 24 times per year, each time with a randomly generated sub-sample (90 %) of  
466 the available observations from each station (10 % removed in 5-day blocks), to further explore the uncertainty.  
467 Emissions and uncertainties were averaged across the 24 individual inversions thereby assuming 100 % correlation  
468 between uncertainties in these separate inversions. 1-year inversions were performed covering the period 2013–2017.

#### 469 **4.6 Regional model and inversion study using NAME-HB for India**

470 To investigate regional emissions from the Indian subcontinent from the samples taken on-board a research aircraft  
471 in June and July 2016 (see Sect. 2.4) we used the NAME-HB inversion method described in Sect. 4.4 and Table S1.  
472 Here, the domain spanned from 6° N to 48° N and from 55° E to 109° E with an altitude up to 19 kilometers and  
473 emissions were estimated as the mean over the 2-month period. As with eastern Asia and Western Europe studies,  
474 the sensitivity of the atmospheric measurements to surface emissions was derived using the NAME model. Back-  
475 trajectories were simulated for each minute of each flight path for up to 30 days backward in time. To account for the  
476 motion of the aircraft, hypothetical air parcels were released from a cuboid whose dimensions were defined as the  
477 change in latitude, longitude and altitude of the aircraft during each 1 minute period, at a release rate of 1000 air  
478 parcels  $\text{min}^{-1}$ . Wherever possible, samples were collected during periods of level flight, to minimise the altitude  
479 component of the release volume. India's a priori emissions were set to 18 % of global *c*-C<sub>4</sub>F<sub>8</sub> emissions (from Sect.  
480 5.2), equal to India's fraction of the global population, but uniformly distributed over India. A large uncertainty was  
481 assigned (Table S1) to reflect the lack of information on India's current *c*-C<sub>4</sub>F<sub>8</sub> emissions. A priori vertical boundary  
482 conditions were assigned using background mole fractions from MHD (N, E and W) and CGO (S). Offsets to these  
483 boundary conditions were estimated in the inversion. Due to the limited number of samples taken onboard the  
484 aircraft, the regional inversion for the Indian subcontinent may have more difficulty identifying individual point  
485 sources (see Section 4.4), which also may not be emitting at all times. We report only emissions for Northern and  
486 Central India (NCI) as the inversion has low sensitivity over southern India and Sri Lanka and the north western edge  
487 of the domain, and no sensitivity beyond the Himalayas (see Fig. S5). Sensitivity tests indicate that *c*-C<sub>4</sub>F<sub>8</sub> emissions  
488 determined for NCI are insensitive to the choice of a priori emissions (see Fig. S6).

#### 489 **4.7 Pollution events at Zeppelin station**

490 The Zeppelin (ZEP) station is located in a clean Arctic environment and receives air masses representative mostly of  
491 the Arctic background. Nevertheless, 10 cases of enhanced *c*-C<sub>4</sub>F<sub>8</sub> mole fractions were observed with the arrival of  
492 air masses from Eurasia. To trace the origin of these events, we used 3-hourly 50-day backward simulations for a  
493 passive tracer with version 10 of the Lagrangian particle dispersion model FLEXPART (Stohl et al., 2005). The  
494 model was driven with operational meteorological analyses of the European Centre for Medium Range Weather  
495 Forecasts (ECMWF, <https://www.ecmwf.int/>). The model set-up was similar to that typically used for inversion  
496 studies (Stohl et al., 2009), but the number of events observed at the station was too small for a sensible regional  
497 inversion. Instead, we inserted unit emission sources ( $\sim 1 \text{ kg s}^{-1}$ ) at two facilities in Russia producing PTFE and  
498 halogenated chemicals including *c*-C<sub>4</sub>F<sub>8</sub> (HaloPolymer, Kirovo-Chepetsk, Kirov Oblast and Galogen Open Joint-  
499 Stock Company, Perm), one or both of which we suspect to be responsible for the observed enhancements. We then  
500 scaled the modeled *c*-C<sub>4</sub>F<sub>8</sub> mole fractions based on these two unit sources to the observed enhancements to estimate  
501 the source strength required to explain the observations. The two sources are quite close to each other and thus very  
502 much correlated so it was impossible to quantify the influence of each source individually, but it turned out that each  
503 source required about the same flux to produce a similar good match with the observations.

## 504 **5 Results and discussion**

### 505 **5.1 Atmospheric histories of *c*-C<sub>4</sub>F<sub>8</sub> in both hemispheres**

506 Figure 1 shows the atmospheric histories of *c*-C<sub>4</sub>F<sub>8</sub> in the extra-tropical NH and SH determined from several sets of  
507 archive measurements and pollution filtered data from six in situ measurement stations. As detailed in Sect. 2.2, the  
508 data shown have gone through an iterative filtering process which mostly removed outliers from the NH record. The  
509 pollution-free monthly mean in situ data for the four extra-tropical NH stations shown here and ZEP agree within  
510 precisions, although JFJ data tends to be at the lower range since early 2015 for unknown reasons. The two extra-  
511 tropical SH stations, CGO and ASA also agree well with each other. Mole fractions measured in both hemispheres  
512 show a clear and consistent interhemispheric gradient reflecting the high precision of the measurements and  
513 indicating that emissions of *c*-C<sub>4</sub>F<sub>8</sub> predominantly occur in the NH. These data form a consistent atmospheric record  
514 of *c*-C<sub>4</sub>F<sub>8</sub> from the late 1970s to 2017 in both hemispheres, albeit with very sparse data for the NH before in situ  
515 measurements started at JFJ and at other NH stations. The inset in Fig. 1 shows that the interhemispheric gradient,  
516 based on in situ measurements at high-latitude stations in the NH (MHD, THD, SIO) and SH (CGO) has been rising  
517 from ~0.05 ppt in 2011 to ~0.09 ppt in 2017, which suggests increasing, predominantly NH, emissions.

518 To augment our *c*-C<sub>4</sub>F<sub>8</sub> data set and to extend our reconstruction further backwards in time, we measured air samples  
519 extracted at several firn sites from both hemispheres and interpreted the data with the CSIRO global inversion  
520 framework. The CSIRO inversion (see Sect. 4.3.1) yields the atmospheric history of *c*-C<sub>4</sub>F<sub>8</sub> starting in 1900 until  
521 present, although abundances are essentially not different from zero (<0.02 ppt) until the early 1960s (Fig. 3).  
522 Average global *c*-C<sub>4</sub>F<sub>8</sub> mole fractions from the CSIRO inversion reached 0.45 ppt in 1980, 0.74 ppt in 1990, 0.97 ppt  
523 in 2000, 1.29 ppt in 2010, and 1.66 ppt in 2017. The Bristol inversion (see Sect. 4.3.2) does not incorporate firn data,  
524 still atmospheric histories of the two inversions generally are in good agreement (see Fig. S7).

525 The CSIRO inversion reconstructs that the global rise rate of *c*-C<sub>4</sub>F<sub>8</sub> accelerated from near zero before the late 1960s  
526 to ~0.03–0.04 ppt yr<sup>-1</sup> in the mid-1970s to late 1980s, after which the rise rate slowed to ~0.02 ppt yr<sup>-1</sup> in the early  
527 1990s to mid-2000s. It increased again in the early 2000s and reached ~0.07 ppt yr<sup>-1</sup> in 2017.

528 Compared to Oram et al. (2012), our work extends the SH record from 2008 until present and, arguably, from 1978  
529 back to 1900. Furthermore, it adds the full NH record. SH mole fractions reconstructed by Oram et al. (2012) are  
530 very similar in 1978 and 1990, but ~0.06 ppt lower in the mid-1980s (~11 %) and the late 1990s to late 2000s (~5 %,  
531 see Fig. S8). Although the stated precision in Oram et al. (2012) of 0.8 % (~0.01 ppt at 1.2 ppt) is similar to the 0.01–  
532 0.02 ppt achieved here, the resulting precisions of the CGAA measurements achieved here are significantly  
533 improved, e.g. the noise in the CGAA reconstruction by Oram et al. (2012) is about as large as the interhemispheric  
534 gradient determined here (see Fig. S8). The estimated accuracy of the SIO-14 *c*-C<sub>4</sub>F<sub>8</sub> calibration scale of ~2 % also  
535 compares favorably to previous calibration scale uncertainties.

### 536 **5.2 Global *c*-C<sub>4</sub>F<sub>8</sub> emissions**

537 Global *c*-C<sub>4</sub>F<sub>8</sub> emissions (Fig. 5 and Supplement) started to increase in the early 1960s (CSIRO inversion) from near  
538 zero to ~1.2 Gg yr<sup>-1</sup> in the late 1970s to the late 1980s. The Bristol inversion initially reconstructs lower emissions,  
539 but the differences are within the estimated uncertainties for the reconstructed histories (see Fig. 5). Afterwards,

540 emissions determined by both inversions declined to  $\sim 0.8$  Gg yr<sup>-1</sup> in the mid-1990s to early 2000s. Since then  
541 emissions kept increasing, reaching  $\sim 2.2$  Gg yr<sup>-1</sup> in 2017. Both inversions reconstruct emissions which are  
542 significantly larger than available bottom-up inventory information (see Sect. 3 and the Supplement), reflecting the  
543 shortcomings of the current UNFCCC reporting requirements and bottom-up inventories.  
544 Emissions presented by Oram et al. (2012) agree very well from 2001 to 2007 with our results and on average also  
545 from 1978 to 2001, although they show larger variability. Global emissions roughly estimated by Harnisch (2000)  
546 based on measurements by Travnicek (1998) of  $\sim 0.7$  Gg yr<sup>-1</sup> from 1978 to 1997 are 30% lower than our estimate of  
547  $1.01 \pm 0.10$  Gg yr<sup>-1</sup>. Saito et al. (2010) estimated global emissions of  $0.6 \pm 0.2$  Gg yr<sup>-1</sup> from January 2006 to  
548 September 2009, about half of our  $1.16 \pm 0.09$  Gg yr<sup>-1</sup> estimate. This difference is likely due to slowly changing *c*-  
549 C<sub>4</sub>F<sub>8</sub> mole fractions in calibration tanks used by NIES (Takuya Saito, personal communication, 2018), which would  
550 significantly affect the background rise rate and thus global emissions, but would have had less influence on the  
551 regional emissions estimated by Saito et al. (2010) as these are mostly dependent on the magnitude of the much  
552 larger pollution events above background.  
553 Global emissions of *c*-C<sub>4</sub>F<sub>8</sub> have clearly not levelled off at 2005–2008 levels as had been suggested by Oram et al.  
554 (2012), but kept rising. In contrast, emissions of other minor PFCs, C<sub>2</sub>F<sub>6</sub> and C<sub>3</sub>F<sub>8</sub>, have decreased since the early  
555 2000s and stabilized in recent years (Trudinger et al., 2016), reflecting that emission sources and/or use patterns of *c*-  
556 C<sub>4</sub>F<sub>8</sub> are different from those of the other minor PFCs. Weighted by GWP<sub>100</sub> (100-year timescale) estimated 2017  
557 emissions of *c*-C<sub>4</sub>F<sub>8</sub>, C<sub>3</sub>F<sub>8</sub>, C<sub>2</sub>F<sub>6</sub>, and CF<sub>4</sub> were 0.021, 0.005, 0.022, and 0.083 billion tonnes of CO<sub>2</sub>-eq., respectively  
558 (see Fig. S9). *c*-C<sub>4</sub>F<sub>8</sub> CO<sub>2</sub>-eq. emissions have been larger than those of C<sub>3</sub>F<sub>8</sub> since 2004 and, assuming continued  
559 growth, will also surpass C<sub>2</sub>F<sub>6</sub> emissions within a year or two, so that *c*-C<sub>4</sub>F<sub>8</sub> will become the second most important  
560 PFC emitted into the global atmosphere in terms of CO<sub>2</sub>-eq. emissions. In the next section, we will investigate  
561 regional emissions of *c*-C<sub>4</sub>F<sub>8</sub> to gain a better understanding how individual regions and sources may contribute to the  
562 global emissions.

### 563 **5.3 Regional *c*-C<sub>4</sub>F<sub>8</sub> emission studies**

#### 564 **5.3.1 Emissions from eastern Asia**

565 Within the AGAGE network, the two stations in eastern Asia, Gosan (GSN) and Shangdianzi (SDZ), show by far the  
566 most frequent and most pronounced pollution events of up to  $\sim 14$  ppt above NH background, indicating significant  
567 regional emissions (see Fig. S10). Therefore, we use a regional inverse method (NAME-HB) to infer the emissions  
568 in this region ( $20^\circ$  N– $50^\circ$  N and  $110^\circ$  E– $160^\circ$  E, see Sect. 4.4). We focus on the observations from GSN as this site  
569 was operated with relatively few interruptions from June 2010 to the end of 2017 and had almost full coverage for  
570 each year from 2011 to 2015. Significantly longer data gaps exist for SDZ, which would have made interpretation of  
571 inversion results more difficult. The sensitivity of the inversion generally decreases with distance to the receptor  
572 station resulting in relatively low sensitivity for emissions from western China, eastern Japan and Taiwan (the  
573 cumulative footprint map for 2010–2017 is shown in Fig. S11). Therefore, we report in Table 2 and Fig. 6 estimated  
574 emissions for eastern China, western Japan, South Korea, North Korea, and Taiwan. *c*-C<sub>4</sub>F<sub>8</sub> emissions in this eastern  
575 Asian domain increased from  $0.36 \pm 0.07$  Gg yr<sup>-1</sup> in 2010 to  $0.73 \pm 0.13$  Gg yr<sup>-1</sup> in 2016 and 2017 and were



576 dominated by emissions from eastern China. The a priori emissions for eastern China of  $0.185 \text{ Gg yr}^{-1}$  are based on  
577 the Saito et al. (2010) estimate for all of China for November 2007 to September 2009, but the inversion suggests  
578 emissions that are  $\sim 62\%$  higher in 2010 and more than triple in 2017. Note, that if we were to sum up emissions for  
579 all regions of China, including those where the inversion has low sensitivity, total emissions would be another  $\sim 50\text{--}$   
580  $75\%$  higher. In contrast, the EDGAR 4.2 emissions inventory, the only available bottom-up information (see Sect. 3  
581 and the Supplement), suggests no significant emissions from China.

582 For western Japan we find emissions of  $\sim 0.02 \text{ Gg yr}^{-1}$  (no trend),  $\sim 30\%$  lower than the a priori emissions (from Saito  
583 et al. 2010, see Sect. 4.4). While total country emissions are likely higher, the available bottom-up information (see  
584 Sect. 3 and Supplement) suggests an order of magnitude lower emissions for all of Japan. For South Korea, the  
585 inversion adjusts emissions down to  $0.01\text{--}0.02 \text{ Gg yr}^{-1}$  in most years and up to  $\sim 0.04 \text{ Gg yr}^{-1}$  in 2014 and 2015.  
586 Except perhaps for 2012 and 2017, emissions from South Korea are significantly higher than the  $0.003\text{--}0.008 \text{ Gg yr}^{-1}$   
587 suggested by the available bottom-up information. Emissions from Taiwan show no trend and are relatively small  
588 with  $\sim 0.01 \text{ Gg yr}^{-1}$ , which is  $\sim 50\%$  of  $\sim 0.02 \text{ Gg yr}^{-1}$  indicated by the Taiwanese NIR, though it should be noted that  
589 the inversion has relatively low sensitivities for some parts of Taiwan (see Fig. S11). Overall, emissions from  
590 western Japan, South Korea, and Taiwan are small, despite their large semiconductor industries (see also Fig. 7),  
591 suggesting that this industry sector is not a major emitter of  $c\text{-C}_4\text{F}_8$ . Emissions from North Korea are also small.

592 Combined regional  $c\text{-C}_4\text{F}_8$  emissions doubled from 2010 to 2016, driven by Chinese emissions. They represent  $31 \pm$   
593  $4\%$  of global emissions (2010–2017), while eastern China’s emissions represent  $28 \pm 4\%$ . The difference between  
594 global and eastern Asian emissions remained relatively consistent, ranging from  $\sim 1.04 \text{ Gg yr}^{-1}$  in 2010 to  $1.47 \text{ Gg yr}^{-1}$   
595  $^1$  in 2017 with an average of  $1.20 \pm 0.14 \text{ Gg yr}^{-1}$  from 2010 to 2017 and  $1.15 \pm 0.03 \text{ Gg yr}^{-1}$  from 2011 to 2015, the  
596 years with the best data coverage at GSN and thus highest confidence in the results. This means that the increase in  
597 global emissions is essentially explained by the increase in eastern Asian emissions, i.e. mostly from China, but also  
598 that significant emissions of  $\sim 1.16 \text{ Gg yr}^{-1}$  exist outside of the investigated region (a fraction of which may stem  
599 from industries located in parts of China and perhaps Japan where the inversion has low sensitivity).

600 Figure 7 shows that from 2010 to 2017 emissions in eastern China occur from the highly industrialized provinces  
601 Shandong, Tianjin, and parts of Henan and Hebei (south/southwest of Beijing) as well as from Shanghai and  
602 neighboring Jiangsu (to the north), Anhui (to the west) and Zhejiang (to the south) in the Yangtze River Delta region.  
603 Also shown are locations of potential industrial  $c\text{-C}_4\text{F}_8$  point sources. For South Korea, western Japan and Taiwan,  
604 semiconductor fabrication plants do not seem to be dominant  $c\text{-C}_4\text{F}_8$  emitters as they are not co-located with large  $c\text{-}$   
605  $\text{C}_4\text{F}_8$  emissions (though the inversion has low sensitivity for eastern Japan, where many more semiconductor  
606 fabrication plants (FABS) and several PTFE and HCFC-22 plants are located, hence emissions from this region  
607 cannot be analyzed).

608 In China, the picture is less clear than in South Korea, Japan and Taiwan, as several semiconductor fabrication plants  
609 in the Yangtze River Delta region are co-located with strong  $c\text{-C}_4\text{F}_8$  emissions, while those near Beijing are not.  
610 Many of the potential production facilities of TFE and HFP monomers and PTFE and FEP polymers are co-located  
611 with areas where strong  $c\text{-C}_4\text{F}_8$  emissions occur. This is consistent with information from the second largest producer  
612 of PTFE in China that they do not recover  $c\text{-C}_4\text{F}_8$  by-product, but do emit  $c\text{-C}_4\text{F}_8$  to the atmosphere (Hu, J., personal  
613 communication, 2018). Still, the two facilities north east of Beijing do not seem to emit  $c\text{-C}_4\text{F}_8$ , perhaps reflecting

614 that some producers minimize  $c\text{-C}_4\text{F}_8$  emissions, e.g. to increase yield or to use  $c\text{-C}_4\text{F}_8$  for other purposes, such as for  
615 the semiconductor industry. Several facilities are also located in provinces for which the inversion has low  
616 sensitivity. Most HCFC-22 production facilities are not co-located with strong  $c\text{-C}_4\text{F}_8$  emissions, while  $\text{CHCl}_3$   
617 production facilities tend to be in areas with  $c\text{-C}_4\text{F}_8$  emissions. This may reflect that  $\text{CHCl}_3$  production has shifted  
618 from use as a feedstock to produce HCFC-22 for dispersive applications (refrigeration or foam blowing), where no  $c\text{-C}_4\text{F}_8$   
619  $\text{C}_4\text{F}_8$  emissions occur, to production of TFE/HFP/PTFE/FEP via HCFC-22 pyrolysis, where  $c\text{-C}_4\text{F}_8$  by-product  
620 emissions occur, perhaps at the same or close-by facilities. This would be consistent with the start of the HCFC  
621 phase-out for dispersive applications in developing countries mandated by the Montreal Protocol on the Protection of  
622 Ozone Layer. Then again,  $\text{CHCl}_3$  has other uses, e.g. as solvent (Tsai, 2017), without any potential  $c\text{-C}_4\text{F}_8$  emissions.  
623 Note, that at one or both of the PTFE production facilities in Zhejiang province (Juhua Group Corporation) HFO-  
624 1234yf is produced since 2016, using a process which starts out with the same chemistry needed for PTFE/FEP  
625 production, that is the pyrolysis of HCFC-22 to TFE and HFP, with  $c\text{-C}_4\text{F}_8$  as potential by-product (see Supplement).  
626 There is no strong correlation between  $c\text{-C}_4\text{F}_8$  emissions distribution and population density, e.g. emissions from  
627 Henan and Hebei provinces are significantly lower than those from Shandong despite similar total population, which  
628 may indicate that combustion of fluoropolymers in waste incineration facilities (Morisaki, 1978; Kannan et al., 2005;  
629 van der Walt et al., 2008; Ji et al., 2016; Bezuidenhoudt et al., 2017) is not a dominant source of  $c\text{-C}_4\text{F}_8$  emissions.  
630 If  $c\text{-C}_4\text{F}_8$  emissions in eastern Asia are predominantly associated with TFE/HFP/PTFE/FEP production via the  
631 pyrolysis of HCFC-22,  $c\text{-C}_4\text{F}_8$  emissions may co-occur with small emissions of TFE and HFP. HFC-23 emissions  
632 may also co-occur as HCFC-22 is produced from  $\text{CHCl}_3$  and HFC-23 is a by-product that in developing countries is  
633 probably again vented to the atmosphere since the UNFCCC Clean Development Mechanism (CDM) funding to  
634 avoid HFC-23 emissions has expired (Simmonds et al., 2018; Say et al., 2019). While the global atmospheric  
635 lifetime of TFE is only  $\sim 2$  days, the lifetime of HFP is  $\sim 6$  days (Acerboni et al., 2001), so that HFP may be  
636 detectable near strong emission sources and serve as a sensitive marker for regional TFE/HFP/PTFE/FEP production.  
637 After adding HFP to the measurements in late 2018, we find that HFP pollution events at SDZ always coincide with  
638  $c\text{-C}_4\text{F}_8$  and HFC-23 pollution events (see Fig. S12 and its caption in the Supplement). HFP pollution events at GSN  
639 are much weaker, reflecting the short atmospheric lifetime and the more distant source region, but they also coincide  
640 with  $c\text{-C}_4\text{F}_8$  and HFC-23 pollution events. At both sites, however,  $c\text{-C}_4\text{F}_8$  pollution events also coincide with  
641 enhancements of other anthropogenic compounds which may just point to generally polluted air in the region, so it is  
642 difficult to draw definitive conclusions. Still it is clear that HFP is emitted in eastern Asia, likely in China, and HFP  
643 as well as  $c\text{-C}_4\text{F}_8$  emissions can be explained by PTFE/FEP production. Measurements of HFP at SIO and ASA,  
644 confirm that it is virtually absent ( $\leq 0.01$  ppt) from the global background atmosphere even in urban environments.  
645 Overall, the strong  $c\text{-C}_4\text{F}_8$  emissions in eastern China and their source regions are consistent with our hypothesis of  
646 emissions from TFE/HFP/PTFE/FEP production facilities due to little or no recovery or abatement of  $c\text{-C}_4\text{F}_8$  by-  
647 product and the significant fraction of global PTFE production (53–67 % in 2015) occurring in China (see Table S3).

### 648 5.3.2 Emissions from North Western Europe

649 Outside of eastern Asia, the TAC station in East Anglia, UK shows by far the most frequent and most pronounced  $c\text{-C}_4\text{F}_8$   
650  $\text{C}_4\text{F}_8$  pollution events of any AGAGE station, with a few reaching  $\sim 5$  to 10 ppt above NH background, indicating

651 close-by emissions. Data from the TAC, MHD, JFJ and CMN stations and the InTEM regional inverse method (see  
652 Sect. 4.5) were used to estimate emissions from North Western Europe (42° N to 59° N and -11° E to 15° E) based  
653 on to the areas of highest sensitivity to the observations (see Fig. S13). Compared to eastern Asia, we find only small  
654 emissions of  $0.026 \pm 0.013 \text{ Gg yr}^{-1}$  (Ireland, UK, France, Germany, Belgium, the Netherlands, Luxemburg, and  
655 Denmark, 2013–2017) without any significant temporal trend, corresponding to only ~1 % of global emissions,  
656 despite an estimated 14 % of global PTFE production in 2015 (see Table S3). The mean distribution of emissions is  
657 shown in Fig. 8. Similar to eastern Asia, many identified semiconductor FABS in Europe are not co-located with *c*-  
658  $\text{C}_4\text{F}_8$  emission hotspots, while several FABS in Northern France, the UK, Ireland, and the Netherlands seem to be co-  
659 located. Producers of PTFE and FEP and facility locations in Europe were determined from company websites  
660 (3M/Dyneon, AGC/Asahi Glass, Arkema, Chemours/DuPont, Saint-Gobin, Solvay) and the European Pollutant  
661 Release and Transfer Register (<https://prtr.eea.europa.eu>), but it is very difficult to determine at which of the many  
662 facilities PTFE or FEP are actually produced and thus where *c*- $\text{C}_4\text{F}_8$  may be emitted. It seems that several facilities in  
663 The Netherlands, Belgium, the UK, France, and Italy which likely produce PTFE are co-located with identified *c*-  
664  $\text{C}_4\text{F}_8$  emission hotspots (Fig. 8). Still, many mismatches exist, reflecting the uncertainties in determining the exact  
665 facility locations, the relatively small emission strength and uncertainties of the inversion. As in eastern Asia, there  
666 seems to be no correlation with population density, which suggests that waste incineration of fluoropolymers is not a  
667 dominant *c*- $\text{C}_4\text{F}_8$  source here either. The inversion is broadly consistent with emissions from TFE/HFP/PTFE/FEP  
668 production and FABS, but emissions from other industrial sources may also play a role. While emissions of  $0.026 \pm$   
669  $0.013 \text{ Gg yr}^{-1}$  are relatively small, it is noteworthy that UNFCCC reporting suggest much smaller *c*- $\text{C}_4\text{F}_8$  emissions  
670 ( $0.0007 \text{ Gg yr}^{-1}$  (UNFCCC, 2013–2014) vs.  $0.0017 \text{ Gg yr}^{-1}$  (bottom-up emission inventories, Section 3, 2013–2014)).

### 671 **5.3.3 Emissions from South Eastern Australia**

672 Other urban locations of the AGAGE network, such as SIO, USA and ASA, Australia show much smaller pollution  
673 events above global background (up to ~2.5 ppt) than those seen at TAC, suggesting even lower emissions. Still, the  
674 few pollution events at ASA and even CGO are interesting as production of PFCs in Australia has never been  
675 recorded. CFC-11, CFC-12, and HCFC-22 were manufactured starting in 1962 at two facilities in Sydney, but  
676 production ceased in 1995 and trace gas emissions from Sydney are rarely if ever observable at CGO or ASA.  
677 Without any currently known fluorocarbon production, any *c*- $\text{C}_4\text{F}_8$  pollution events observed at CGO or ASA should  
678 not be due to fugitive emissions. *c*- $\text{C}_4\text{F}_8$  imports to Australia are ~4 to 50  $\text{kg yr}^{-1}$  (2011–2015), likely for minor  
679 refrigeration uses. In contrast, small but identifiable *c*- $\text{C}_4\text{F}_8$  pollution episodes at CGO suggest Melbourne emissions  
680 of ~2  $\text{t yr}^{-1}$  ( $0.002 \text{ Gg yr}^{-1}$ ) in 2016 (down from ~5  $\text{t yr}^{-1}$  in 2009, Inter Species Correlation method, ISC, c.f., Fraser  
681 et al., 2014; Dunse et al., 2018). Scaled by population to Australia (for lack of a better proxy), emissions from 2009  
682 to 2016 could be ~10–25  $\text{t yr}^{-1}$  ( $0.01\text{--}0.025 \text{ Gg yr}^{-1}$ ), 2–3 orders of magnitude higher than import data suggests. Since  
683 early 2017, HFP has been measured at ASA (see Fig. S12 caption). Occasional, small HFP pollution events, which  
684 are often, but not always, associated with *c*- $\text{C}_4\text{F}_8$  pollution events, may point to small scale production of  
685 TFE/HFP/PTFE/FEP in Melbourne or perhaps these small emissions stem from incineration of waste containing  
686 fluoropolymers. Another possible explanation could be that more *c*- $\text{C}_4\text{F}_8$  is imported in products for minor  
687 applications than identified in import data due to inadequate labelling. On a global scale, estimated Australian *c*- $\text{C}_4\text{F}_8$

688 emissions of  $\sim 0.015 \text{ Gg yr}^{-1}$  are small,  $\sim 0.7 \%$  of global emissions. PFC ( $\text{CF}_4$ ,  $\text{C}_2\text{F}_6$ ) pollution episodes at Cape Grim  
689 and Aspendale due to PFC emissions from South Eastern Australian aluminum smelters (Portland and Pt. Henry,  
690 Victoria and Bell Bay, Tasmania) do not show any evidence of  $c\text{-C}_4\text{F}_8$  emissions (Fraser et al., 2013; CSIRO  
691 unpublished data).

#### 692 **5.3.4 Emissions from under-sampled regions such as the US, India, Russia**

693 The AGAGE network does not closely monitor large areas of the globe where  $c\text{-C}_4\text{F}_8$  emissions may occur. For  
694 example, many semiconductor FABs are located in the western, southern, and eastern US and chemical facilities  
695 located in the southern and eastern US are estimated to account for  $\sim 10 \%$  of global PTFE production in 2015, while  
696 facilities in India and Russia are estimated to account for  $\sim 8 \%$  and  $\sim 6 \%$ , respectively (see Tables S3 and S4). The  
697 two AGAGE stations in California are only able to capture a fraction of these emissions due to predominant westerly  
698 winds and therefore we cannot estimate  $c\text{-C}_4\text{F}_8$  emissions from the continental US. If PTFE production facilities in  
699 the US are operated as in NW Europe, emissions should be similarly small. If facilities in India and Russia are  
700 operated as in China, emissions could be significant as well. In the case of Russia this seems likely as the original  
701 technology for fluoropolymer production in China apparently stems from Russia (Buznik, 2009).

#### 702 **5.3.5 Emissions from India**

703 Say et al. (2019) recently presented measurements from an aircraft campaign in June and July 2016 (see Sect. 2.4)  
704 over the Indian subcontinent to determine emissions of ODS and HFCs. Here we use their  $c\text{-C}_4\text{F}_8$  measurements and  
705 the NAME-HB inversion (see Sect. 4.6) and estimate emissions of  $0.14 (0.09\text{--}0.20) \text{ Gg yr}^{-1}$  for Northern and Central  
706 India (NCI). Data are only available for two months in 2016, but seasonality in industrial emissions of  $c\text{-C}_4\text{F}_8$  is not  
707 expected. Given the limitations of the inversion method to identify distant point sources from a relatively small  
708 number of samples (see Sections 4.4 and 4.6), the posterior emissions distribution (Fig. 9) is consistent with  
709 emissions from facilities producing PTFE. Several of the HCFC-22 production facilities are co-located or very close  
710 to these PTFE producing facilities, suggesting that a fraction of HCFC-22 is pyrolyzed to produce monomers for  
711 PTFE and FEP. Two HCFC-22 production facilities are outside of areas with strong  $c\text{-C}_4\text{F}_8$  emissions, possibly  
712 because these two sites focus on production of HCFC-22 for dispersive applications (refrigeration or foam blowing),  
713 where no  $c\text{-C}_4\text{F}_8$  emissions occur. The single FAB in India we are aware of is not co-located with significant  $c\text{-C}_4\text{F}_8$   
714 emissions. As in eastern Asia and North Western Europe, there is no apparent correlation of  $c\text{-C}_4\text{F}_8$  emissions with  
715 population density. Emissions predominantly occur outside of the Indo-Gangetic plain, the most densely populated  
716 region of India, which excludes potential sources that scale with population. Instead the inversion allocates emissions  
717 in a much less densely populated region in which multiple likely industrial point sources for  $c\text{-C}_4\text{F}_8$  are located. The  
718 derived emissions account for  $6.8 (4.4\text{--}9.7) \%$  of global  $c\text{-C}_4\text{F}_8$  emissions in 2016, in comparison to the estimated  $\sim 8$   
719  $\%$  of 2015 global PTFE production capacity (see Table S3). While we cannot categorically exclude an unknown  
720 industrial source, these results are consistent with the chemistry of TFE/HFP/PTFE/FEP production as dominant  $c\text{-C}_4\text{F}_8$   
721  $\text{C}_4\text{F}_8$  emission source. Note, that one of the facilities in western India (Navin Fluorine International, Surat, Gujarat) is  
722 known to also produce HFO-1234yf since 2016, using a process which starts out with the same chemistry, that is the  
723 pyrolysis of HCFC-22 to TFE and HFP, with  $c\text{-C}_4\text{F}_8$  as potential by-product (see Supplement). All known Indian

724 PTFE manufacturers are located within the NCI domain, hence the estimated emissions are likely to be roughly  
725 representative of India's national total, though further atmospheric measurements would be required to confirm this.

### 726 **5.3.6 Emissions from facilities in Russia**

727 Measurements at the ZEP site in remote Svalbard show ten small *c*-C<sub>4</sub>F<sub>8</sub> pollution events above NH background of  
728 up to ~0.4 ppt. FLEXPART backward simulations could trace some of these events to two facilities in Russia which  
729 produce PTFE and halogenated chemicals including *c*-C<sub>4</sub>F<sub>8</sub> itself (HaloPolymer, Kirovo-Chepetsk, Kirov Oblast and  
730 Galogen Open Joint-Stock Company, Perm). Figure S14 shows the FLEXPART footprint emission sensitivity map  
731 for the largest observed *c*-C<sub>4</sub>F<sub>8</sub> enhancement on November 19, 2016, suggesting direct transport from the two sites.  
732 The emission sensitivity maps indicate that for six of the ten observed pollution events the air had clearly passed over  
733 one or both of these two sources, even though the timing of the observed events was often not well matched by the  
734 model, which was sometimes off by up to about half a day. While this is not surprising given the large distance  
735 between the source and the receptor, it means that the two sources could not be clearly separated, especially since the  
736 FLEXPART emission sensitivity often also covered both sites for the same arrival times at ZEP. Assuming a unit  
737 emission at those two locations and scaling the resulting simulated mole fractions at ZEP to the observed  
738 enhancements above background, we estimated the emission strength for the two sites together for each event (see  
739 Sect. 4.7). Five of the ten pollution events could be approximately reproduced by this method and required a flux of  
740  $0.18 \pm 0.06$  Gg yr<sup>-1</sup>, while the sixth event required ~0.54 Gg yr<sup>-1</sup>. Averaged for all six events  $0.24 \pm 0.15$  Gg yr<sup>-1</sup>  
741 would be required. Either of these fluxes would be significant, representing  $9 \pm 3$  %, 26 %, and  $12 \pm 7$  % of global  
742 emissions, respectively, compared to ~6 % of estimated global PTFE production in Russia. The uncertainty of this  
743 estimate is large because only a few events were observed and not all of them were reproduced equally well by  
744 FLEXPART. Similar to eastern Asia, the largest *c*-C<sub>4</sub>F<sub>8</sub> pollution event also showed enhancements of HFC-23,  
745 pointing to TFE/HFP/PTFE chemistry as source (see Fig. S15), but other halogenated compounds were also elevated.

## 746 **6 Summary and conclusions**

747 We determine the atmospheric histories of *c*-C<sub>4</sub>F<sub>8</sub> (PFC-318, perfluorocyclobutane) in both hemispheres based on  
748 measurements of archived, in situ, and firm air samples in conjunction with the CSIRO firm model, the AGAGE 12-  
749 box model, and two global inversion frameworks. Compared to previous studies, our work extends the Southern  
750 Hemisphere record from 1978 back to 1900 and from 2008 until 2017 and adds a Northern Hemisphere record, all  
751 reported with improved precisions for air archive measurements (~1–2 %) and a lower uncertainty (2 %) of the SIO-  
752 14 gravimetric calibration scale. We find global *c*-C<sub>4</sub>F<sub>8</sub> atmospheric mole fractions near zero (< 0.02 ppt) from 1900  
753 until the early 1960s, after which they rose sharply, reaching 0.45 ppt in 1980, 0.74 ppt in 1990, 0.97 ppt in 2000,  
754 1.29 ppt in 2010, and 1.66 ppt in 2017. Global *c*-C<sub>4</sub>F<sub>8</sub> emissions started to increase in the 1960s from near zero to  
755  $\sim 1.2 \pm 0.1$  (1 $\sigma$ ) Gg yr<sup>-1</sup> in the late 1970s to the late 1980s. After this, emissions declined to  $\sim 0.77 \pm 0.03$  Gg yr<sup>-1</sup> in  
756 the mid-1990s to early 2000s. After this emissions again increased, reaching  $\sim 2.20 \pm 0.05$  Gg yr<sup>-1</sup> in 2017. These  
757 global emissions are significantly larger than what can be compiled from available bottom-up inventory information  
758 ( $70 \pm 17$  times, 1990–1996,  $29 \pm 5$  times, 1997–2010,  $15 \pm 1$  times, 2011–2014).

759 Using the NAME-HB regional inverse method and observations at Gosan station we find that emissions from eastern  
760 Asia rose from  $\sim 0.36$  Gg yr<sup>-1</sup> in 2010 to  $\sim 0.73$  Gg yr<sup>-1</sup> in 2016 and 2017, representing  $31 \pm 4$  % of global emissions,  
761 predominantly from eastern China. Strong *c*-C<sub>4</sub>F<sub>8</sub> emissions are found from heavily industrialized provinces  
762 south/southwest of Beijing and near the Yangtze River Delta. In contrast, emissions from western Japan, South  
763 Korea, and Taiwan are small, suggesting that their large semiconductor industries are not major *c*-C<sub>4</sub>F<sub>8</sub> emitters.  
764 While we cannot categorically exclude emissions from other industrial sources, overall, the strong *c*-C<sub>4</sub>F<sub>8</sub> emissions  
765 in eastern China and their spatial pattern are roughly consistent with emissions from production of  
766 TFE/HFP/PTFE/FEP and other fluorochemicals. A significant fraction of global PTFE production (53–67 % in 2015)  
767 occurs in China and, as indicated by the second largest producer of PTFE in China, the *c*-C<sub>4</sub>F<sub>8</sub> by-product from the  
768 underlying HCFC-22 pyrolysis process is not recovered or abated, but rather emitted to the atmosphere.

769 Based on samples collected over the Indian subcontinent in mid-2016, we determine emissions of 0.14 (0.09–0.20)  
770 Gg yr<sup>-1</sup> *c*-C<sub>4</sub>F<sub>8</sub> from Northern and Central India (NCI),  $\sim 6.8$  (4.4–9.7) % of global emissions. Within the limitations  
771 of the inversion, the determined emission map is also roughly consistent with emissions from TFE/PTFE production.  
772 Using the InTEM regional inverse method and measurements at four western European stations, we only find small  
773 NW European emissions of  $\sim 0.02 \pm 0.01$  Gg yr<sup>-1</sup> *c*-C<sub>4</sub>F<sub>8</sub> from 2013–2017 ( $\sim 1$  % of global emissions), in contrast to  
774 an estimate of 14 % of global PTFE production capacity in 2015. The inversion also points to facilities which may  
775 produce PTFE and FEP and semiconductor fabrication plants though the picture is less clear.

776 No obvious correlation between population density and *c*-C<sub>4</sub>F<sub>8</sub> emissions is found in Eastern Asia, NCI, and NW  
777 Europe, indicating that incineration of waste containing fluoropolymers is not a major source of *c*-C<sub>4</sub>F<sub>8</sub>.

778 Based on data from two Australian stations and an Inter Species Correlation method, Australian *c*-C<sub>4</sub>F<sub>8</sub> emissions are  
779 estimated to be small, perhaps  $\sim 0.7$  % of global *c*-C<sub>4</sub>F<sub>8</sub> emissions. We find no evidence for *c*-C<sub>4</sub>F<sub>8</sub> production from  
780 three large aluminum smelters in SE Australia.

781 Based on a few *c*-C<sub>4</sub>F<sub>8</sub> pollution events observed at Zeppelin station and a rough FLEXPART analysis, we estimate  
782 that emissions from two Russian facilities known to produce PTFE and halocarbons including *c*-C<sub>4</sub>F<sub>8</sub> itself could be  
783  $\sim 0.24 \pm 0.15$  Gg yr<sup>-1</sup>. While this could represent a significant fraction of global emissions (possibly ranging from 5 to  
784 26 %), uncertainties are very large.

785 In summary, for the year 2016, we find global *c*-C<sub>4</sub>F<sub>8</sub> emissions of  $2.06 \pm 0.10$  Gg yr<sup>-1</sup>, with  $0.73 \pm 0.12$  Gg yr<sup>-1</sup> from  
786 parts of eastern Asia (36 % of the global total), 0.14 (0.09–0.20) Gg yr<sup>-1</sup> from Northern and Central India (6.8 %),  
787  $\sim 0.024 \pm 0.013$  Gg yr<sup>-1</sup> from North Western Europe ( $\sim 1$  %), and  $\sim 0.015$  Gg yr<sup>-1</sup> from Australia ( $\sim 0.7$  %).

788 Current monitoring capabilities of the AGAGE network leave large areas with potential *c*-C<sub>4</sub>F<sub>8</sub> emission sources un-  
789 or under-monitored, e.g. most of the U.S., India, Russia, western China, and eastern Japan, where various  
790 semiconductor facilities and fluorochemical and fluoropolymer production plants are located.

791 While many possible uses and emission sources of *c*-C<sub>4</sub>F<sub>8</sub> are found in the literature and though we cannot  
792 categorically exclude unknown industrial sources, the start of significant *c*-C<sub>4</sub>F<sub>8</sub> emissions around the 1960s may  
793 well be related to the initial synthesis of PTFE in 1938 with commercial production of PTFE (“Teflon”) by DuPont  
794 commencing in 1947 (Gangal and Brothers, 2015) via pyrolysis of HCFC-22, with *c*-C<sub>4</sub>F<sub>8</sub> as a by-  
795 product/intermediate. It seems unlikely that process control or abatement to minimize *c*-C<sub>4</sub>F<sub>8</sub> by-production were in  
796 place in the early decades of PTFE production and *c*-C<sub>4</sub>F<sub>8</sub> by-product was probably emitted to the atmosphere,

797 explaining the steep increase in global emissions reconstructed here. With the advent of UNFCCC by-product  
798 reporting requirements in the 1990s, concern about climate change and product stewardship, abatement, and perhaps  
799 collection of *c*-C<sub>4</sub>F<sub>8</sub> for use in the semiconductor industry where it can be easily abated, it is conceivable that fugitive  
800 *c*-C<sub>4</sub>F<sub>8</sub> in developed countries (UNFCCC Annex 1) overall were reduced, explaining the observed stabilization and  
801 reduction of global emissions in the 1980s and 1990s. Similar efforts to contain and destroy by-product emissions of  
802 fluorocarbons, e.g. HFCs, from the 1980s to the 2000s are documented in the Toxics Release Inventory ([https://](https://www.epa.gov/toxics-release-inventory-tri-program)  
803 [www.epa.gov/toxics-release-inventory-tri-program](https://www.epa.gov/toxics-release-inventory-tri-program)) Program of the US EPA and the European Pollutant Release and  
804 Transfer Register. Concurrently, production of PTFE in China increased rapidly, e.g. from 2000 to 2005 by ~26 %  
805 yr<sup>-1</sup>, followed by a slowdown to ~14% yr<sup>-1</sup> from 2005 to 2015 and perhaps ~8 % yr<sup>-1</sup> from 2015 onward, reaching an  
806 estimated 53–67 % of global production in 2015 (see Tables S2, 3, and 4). Without any emission reduction  
807 requirements, it is conceivable that fugitive emissions of *c*-C<sub>4</sub>F<sub>8</sub> from TFE/HFP/PTFE/FEP production in China, and  
808 other developing (UNFCCC non-Annex 1) countries, today dominate global emissions. The 2010 to 2016 rise in rates  
809 of eastern Chinese (eastern Asian) *c*-C<sub>4</sub>F<sub>8</sub> emissions of ~15 % yr<sup>-1</sup> (~13 % yr<sup>-1</sup>) determined here are compatible to  
810 these PTFE production increase rates of 14 to 8 % yr<sup>-1</sup> in China. Barring other developments, we predict that *c*-C<sub>4</sub>F<sub>8</sub>  
811 emissions will continue to rise and that *c*-C<sub>4</sub>F<sub>8</sub> will become the second most important PFC emitted to the global  
812 atmosphere in terms of CO<sub>2</sub>-eq. emissions within a year or two. While the 2017 radiative forcing of *c*-C<sub>4</sub>F<sub>8</sub> (~0.52  
813 mW m<sup>-2</sup>) is very small compared to that of CO<sub>2</sub>, emissions *c*-C<sub>4</sub>F<sub>8</sub> and other perfluorinated compounds with similarly  
814 long lifetimes and high radiative efficiencies essentially permanently alter the radiative budget of Earth. The fact that  
815 significant emissions of ~1.16 Gg yr<sup>-1</sup> of global emissions (56 %) exist outside of the monitored regions clearly  
816 shows that observational capabilities and reporting requirements need to be improved to understand global and  
817 country-wide emissions of PFCs and other synthetic greenhouse gases and ozone depleting substances.

## 818 **7 Author contributions**

819 JM contributed to archive, firm, and in situ measurements, interpreted the data, and prepared the manuscript with  
820 contributions from all co-authors. CMT provided CSIRO firm model and CSIRO global inversion results and  
821 interpretation. MR provided Bristol global inversion results. LMW provided NAME-HB model runs and emission  
822 estimated for East Asia, DS and ALG provided the same for India. AJM and LMW provided InTEM model runs and  
823 emissions for Europe. AS and NE provided FLEXPART model runs and guided estimation of Russian emissions. DS  
824 and ALG provided the aircraft data from India. CMT, MR, LMW, AJM, DS, ALG, AS, and PJF contributed  
825 significantly to the text. LPS, DJI, TA, JM, PJF, PBK provided and oversaw CSIRO air archive and NH archive  
826 measurements. MKV, SP, SL, M-KP, COJ, LPS, PBK, SOD, PGS, DY, PBK, KMS, OH, BM, CL, JK, JA, MM, SR,  
827 and BY oversaw station operations and provided quality controlled measurement data. PJF provided the estimate of  
828 Australian emissions. CMH provided gravimetric calibration and calibration propagation for the whole AGAGE  
829 network. PKS wrote the software to run all instruments and analyze all measurement data. MKV, BH, CB, VP,  
830 DME, and JS provided firm data and were instrumental in their interpretation. AMcC provided insight into UNFCCC  
831 reporting and bottom-up inventories as well as industrial processes. EM and MC greatly helped with the gathering of  
832 locations of semiconductor facilities. RGP and RFW provided overall project oversight.

833 **8 Acknowledgments**

834 Development of the Medusa GC/MS systems, calibrations, and measurements at the Scripps Institution of  
835 Oceanography, La Jolla as well as operations of Trinidad Head, CA were carried out as part of the international  
836 AGAGE research program and supported by the NASA Upper Atmospheric Research Program in the US with grants  
837 NNX07AE89G and NNX16AC98G to MIT, NNX07AF09G, NNX07AE87G, NNX16AC96G, and NNX16AC97G  
838 to SIO. In the UK, the Department for Business, Energy & Industrial Strategy (BEIS) provided support through  
839 contract 1028/06/2015 to the University of Bristol for Mace Head, Ireland, for Tacolneston, UK and to the UK Met  
840 Office for InTEM analysis. The National Oceanic and Atmospheric Administration (NOAA) in the US provided  
841 support to the University of Bristol for operations at Ragged Point, Barbados through contract RA-133-R15-CN-  
842 0008 and supported operations at Cape Matatula, American Samoa. Operations in Australia were supported by the  
843 Commonwealth Scientific and Industrial Research Organization (CSIRO), the Bureau of Meteorology (Australia),  
844 the Department of Environment and Energy (Australia), and Refrigerant Reclaim Australia. Operations at  
845 Jungfraujoch were supported by the Swiss National Program HALCLIM/CLIMGAS-CH (Swiss Federal Office for  
846 the Environment, FOEN) and by the International Foundation High Altitude Research Stations Jungfraujoch and  
847 Gornergrat (HFSJG). Operations at Zeppelin were supported by the Norwegian Environment Agency. Operations at  
848 Monte Cimone were supported by the National Research Council of Italy and the Italian Ministry of Education,  
849 University and Research through the Project of National Interest Nextdata. Operations at Gosan were supported by  
850 the National Strategic Project-Fine particle of the National Research Foundation of Korea (NRF) funded by the  
851 Ministry of Science and ICT (MSIT), the Ministry of Environment (ME), and the Ministry of Health and  
852 Welfare(MOHW) (No. NRF-2017M3D8A1092225). Operations at Shangdianzi were supported by the National  
853 Nature Science Foundation of China (41575114). We are indebted to the staff and scientists at AGAGE and other  
854 sites for their continuing contributions to produce high quality measurements of atmospheric trace gases. Firm air  
855 sampling at Law Dome was supported by the Australian Antarctic Division, Australian Antarctic Science Program,  
856 and Australia's Nuclear Science and Technology Organisation. We acknowledge the members of the firm air  
857 sampling teams at South Pole in 2001 and at NEEM in 2008. Firm air sampling at Summit station was supported  
858 through NSF grants ARC-1203779 and ARC-1204084, with airlift support from the 109th New York Air National  
859 guard. We thank E. J. Dlugokencky and the National Oceanic and Atmospheric Administration (NOAA) Earth  
860 System Research Laboratory (ESRL) Global Monitoring Division (GMD) Carbon Cycle Greenhouse Gases (CCGG)  
861 group for measurements which were instrumental for characterizing the Summit13 firm site. We also thank C.D.  
862 Keeling (deceased) and R.F. Keeling (SIO) for air samples. We thank Dr. T. Saito for helpful discussions. Matthew  
863 Rigby was supported in part by advanced research fellowships from the UK Natural Environment Research Council  
864 (NERC, NE/1021365/1). Luke Western was supported by NERC grant NE/M014851/1. Anita L. Ganesan was  
865 funded under a NERC Independent Research Fellowship (NE/L010992/1). We acknowledge the contribution of  
866 NERC, the Ministry of Earth Sciences, Government of India and the Principal Investigators of 'Drivers of the South  
867 Asian Monsoon' aircraft campaign in India. Funding for the measurements used here were made possible by NERC  
868 grant NE/I027282/1. We thank two anonymous reviewers for their very helpful comments.



869 **References**

- 870 Acerboni, G., Beukes, J. A., Jensen, N. R., Hjorth, J., Myhre, G., Nielsen, C. J., and Sundet, J. K.:  
871 Atmospheric degradation and global warming potentials of three perfluoroalkenes, *Atmos.*  
872 *Environ.*, 35, 24, 4113-4123, 10.1016/S1352-2310(01)00209-6, 2001.
- 873 Adolph, A. C., and Albert, M. R.: Gas diffusivity and permeability through the firn column at  
874 Summit, Greenland: measurements and comparison to microstructural properties, *The*  
875 *Cryosphere*, 8, 1, 319-328, 10.5194/tc-8-319-2014, 2014.
- 876 Arnold, T., Mühle, J., Salameh, P. K., Harth, C. M., Ivy, D. J., and Weiss, R. F.: Automated  
877 measurement of nitrogen trifluoride in ambient air, *Anal. Chem.*, 84, 11, 4798-4804,  
878 10.1021/ac300373e, 2012.
- 879 Arnold, T., Manning, A. J., Kim, J., Li, S., Webster, H., Thomson, D., Mühle, J., Weiss, R. F.,  
880 Park, S., and O'Doherty, S.: Inverse modelling of CF<sub>4</sub> and NF<sub>3</sub> emissions in East Asia, *Atmos.*  
881 *Chem. Phys.*, 18, 18, 13305-13320, 10.5194/acp-18-13305-2018, 2018.
- 882 Aydin, M., Saltzman, E. S., De Bruyn, W. J., Montzka, S. A., Butler, J. H., and Battle, M.:  
883 Atmospheric variability of methyl chloride during the last 300 years from an Antarctic ice core  
884 and firn air, *Geophys. Res. Lett.*, 31, 2, L02109, 10.1029/2003GL018750, 2004.
- 885 Battle, M., Bender, M., Sowers, T., Tans, P. P., Butler, J. H., Elkins, J. W., Ellis, J. T., Conway,  
886 T., Zhang, N., Lang, P., and Clarke, A. D.: Atmospheric gas concentrations over the past century  
887 measured in air from firn at the South Pole, *Nature*, 383, 6597, 231-235, 1996.
- 888 Bezuidenhout, A., Sonnendecker, P. W., and Crouse, P. L.: Temperature and pressure effects on  
889 the product distribution of PTFE pyrolysis by means of qualitative, in-line FTIR analysis, *Polym.*  
890 *Degrad. Stab.*, 142, 79-88, 10.1016/j.polymdegradstab.2017.05.025, 2017.
- 891 Broyer, E., Bekker, A. Y., and Ritter, A. B.: Kinetics of the pyrolysis of chlorodifluoromethane,  
892 *Ind. Eng. Chem. Res.*, 27, 1, 208-211, 10.1021/ie00073a039, 1988.
- 893 Buizert, C., Martinerie, P., Petrenko, V. V., Severinghaus, J. P., Trudinger, C. M., Witrant, E.,  
894 Rosen, J. L., Orsi, A. J., Rubino, M., Etheridge, D. M., Steele, L. P., Hogan, C., Laube, J. C.,  
895 Sturges, W. T., Levchenko, V. A., Smith, A. M., Levin, I., Conway, T. J., Dlugokencky, E. J.,  
896 Lang, P. M., Kawamura, K., Jenk, T. M., White, J. W. C., Sowers, T., Schwander, J., and Blunier,  
897 T.: Gas transport in firn: multiple-tracer characterisation and model intercomparison for NEEM,  
898 Northern Greenland, *Atmos. Chem. Phys.*, 12, 9, 4259-4277, 10.5194/acp-12-4259-2012, 2012.
- 899 Buznik, V. M.: Fluoropolymer chemistry in Russia: Current situation and prospects, *Russ. J. Gen.*  
900 *Chem.*, 79, 3, 520-526, 10.1134/s1070363209030335, 2009.
- 901 Cai, B., Liu, H., Kou, F., Yang, Y., Yao, B., Chen, X., Wong, D. S., Zhang, L., Li, J., Kuang, G.,  
902 Chen, L., Zheng, J., Guan, D., and Shan, Y.: Estimating perfluorocarbon emission factors for  
903 industrial rare earth metal electrolysis, *Resources, Conservation and Recycling*, 136, 315-323,  
904 10.1016/j.resconrec.2018.04.018, 2018.

905 Chinoy, P. B., and Sunavala, P. D.: Thermodynamics and kinetics for the manufacture of  
906 tetrafluoroethylene by the pyrolysis of chlorodifluoromethane, *Ind. Eng. Chem. Res.*, 26, 7, 1340-  
907 1344, 10.1021/ie00067a013, 1987.

908 Christophorou, L. G., and Olthoff, J. K.: Electron interactions with  $c\text{-C}_4\text{F}_8$ , *J. Phys. Chem. Ref.*  
909 *Data*, 30, 2, 449-473, 2001.

910 Chung, M. O., and Bai, C.: Thermodynamic property variation of nonazeotropic refrigerant  
911 mixtures (NARMs) in the temperature gliding zone, *Chemical Engineering Communications*,  
912 180, 1, 1-17, 10.1080/00986440008912199, 2000.

913 Cunnold, D. M., Prinn, R. G., Rasmussen, R. A., Simmonds, P. G., Alyea, F. N., Cardelino, C.  
914 A., Crawford, A. J., Fraser, P. J., and Rosen, R. D.: The Atmospheric Lifetime Experiment, 3.  
915 Lifetime Methodology and Application to 3 Years of  $\text{CFC1}_3$  Data, *J. Geophys. Res.*, 88, C13,  
916 8379-8400, 1983.

917 Cunnold, D. M., Weiss, R. F., Prinn, R. G., Hartley, D., Simmonds, P. G., Fraser, P. J., Miller, B.,  
918 Alyea, F. N., and Porter, L.: GAGE/AGAGE measurements indicating reductions in global  
919 emissions of  $\text{CCl}_3\text{F}$  and  $\text{CCl}_2\text{F}_2$  in 1992-1994, *J. Geophys. Res.*, 102, D1, 1259-1269, 1997.

920 Cunnold, D. M., Steele, L. P., Fraser, P. J., Simmonds, P. G., Prinn, R. G., Weiss, R. F., Porter, L.  
921 W., O'Doherty, S., Langenfelds, R. L., Krummel, P. B., Wang, H. J., Emmons, L., Tie, X. X., and  
922 Dlugokencky, E. J.: In situ measurements of atmospheric methane at GAGE/AGAGE sites during  
923 1985-2000 and resulting source inferences, *J. Geophys. Res.*, 107, D14, 10.1029/2001JD001226,  
924 2002.

925 Dunse, B. L., Derek, N., Fraser, P. J., Krummel, P. B., and Steele, L. P.: Australian and global  
926 HFC, PFC, sulfur hexafluoride nitrogen trifluoride and sulfuryl fluoride emissions, Report  
927 prepared for Australian Government Department of the Environment and Energy, CSIRO Oceans  
928 and Atmosphere, Aspendale, Australia, iv, 33 pp.  
929 <http://www.environment.gov.au/protection/ozone/publications/csiro-report-australian-global-sgg>,  
930 2018.

931 Engel, A., M. Rigby (Lead Authors), Burkholder, J. B., Fernandez, R. P., Froidevaux, L., Hall, B.  
932 D., Hossaini, R., Saito, T., Vollmer, M. K., B. Yao (Coauthors), Altas, E., Bernath, P., Blake, D.  
933 R., Dutton, G., Krummel, P., Laube, J. C., Mahieu, E., Montzka, S. A., Mühle, J., Nedoluha, G.,  
934 O'Doherty, S. J., Oram, D. E., Pfeilsticker, K., Prinn, R. G., Quack, B., Simpson, I. J., R.F. Weiss  
935 (Contributors), Liang, Q., and S. Reimann (Review Editors): Update on Ozone-Depleting  
936 Substances (ODSs) and Other Gases of Interest to the Montreal Protocol (Chapter 1), in:  
937 Scientific Assessment of Ozone Depletion: 2018, Global Ozone Research and Monitoring  
938 Project–Report No. 58, World Meteorological Organization, Geneva, Switzerland, 2018.

939 Fraser, P., Steele, P., and Cooksey, M.: PFC and Carbon Dioxide Emissions from an Australian  
940 Aluminium Smelter Using Time-Integrated Stack Sampling and GC-MS, GC-FID Analysis, in:  
941 *Light Metals 2013*, John Wiley & Sons, Inc., 871-876, 2013.

942 Fraser, P. J., Dunse, B. L., Manning, A. J., Walsh, S., Wang, R. H. J., Krummel, P. B., Steele, L.  
943 P., Porter, L. W., Allison, C., O'Doherty, S., Simmonds, P. G., Mühle, J., Weiss, R. F., and Prinn,

- 944 R. G.: Australian carbon tetrachloride emissions in a global context, *Environ. Chem.*, 11, 1, 77-  
945 88, 10.1071/EN13171, 2014.
- 946 Fraser, P. J., Pearman, G. I., and Derek, N.: CSIRO Non-carbon Dioxide Greenhouse Gas  
947 Research. Part 1: 1975-90, *Hist. Rec. Aust. Sci.*, 29, 1, 1-13, 10.1071/HR17016, 2018.
- 948 Fuller, E. N., Schettler, P. D., and Giddings, J. C.: A new method for prediction of binary gas-  
949 phase diffusion coefficients, *Industrial & Engineering Chemistry*, 58, 5, 18-27,  
950 10.1021/ie50677a007, 1966.
- 951 Ganesan, A. L., Rigby, M., Zammit-Mangion, A., Manning, A. J., Prinn, R. G., Fraser, P. J.,  
952 Harth, C. M., Kim, K. R., Krummel, P. B., Li, S., Mühle, J., O'Doherty, S. J., Park, S., Salameh,  
953 P. K., Steele, L. P., and Weiss, R. F.: Characterization of uncertainties in atmospheric trace gas  
954 inversions using hierarchical Bayesian methods, *Atmos. Chem. Phys.*, 14, 8, 3855-3864,  
955 10.5194/acp-14-3855-2014, 2014.
- 956 Gangal, S. V., and Brothers, P. D.: Perfluorinated Polymers, in: *Kirk-Othmer Encyclopedia of*  
957 *Chemical Technology*, 2015.
- 958 Harnisch, J., Wing, I. S., Jacoby, H. D., and Prinn, R. G.: Primary Aluminum Production: Climate  
959 Policy, Emissions and Costs, Massachusetts Institute of Technology, Report #44, 1998.
- 960 Harnisch, J.: Reactive Fluorine Compounds, in: *Reactive Halogen Compounds in the Atmosphere*  
961 *Vol. 4 Part E, The Handbook of Environmental Chemistry*, Springer Berlin/Heidelberg, 81-111,  
962 1999.
- 963 Harnisch, J.: Atmospheric perfluorocarbons: sources and concentrations, in: *Non-CO<sub>2</sub> greenhouse*  
964 *gases: scientific understanding, control and implementation*, edited by: Ham, J. v., Baede, A.,  
965 Meyer, L., and Ybema, R., Kluwer Academic Publishers, Netherlands, 205-210, 2000.
- 966 Hastings, W. K.: Monte Carlo sampling methods using Markov chains and their applications,  
967 *Biometrika*, 57, 1, 97-109, 10.1093/biomet/57.1.97, 1970.
- 968 Holliday, R. D., and Henry, J. L.: Anode polarization fluorocarbon formation in aluminum  
969 reduction cells, *J. Ind. Eng. Chem.*, 51, 10, 1289-1292, 1959.
- 970 Ivy, D. J., Arnold, T., Harth, C. M., Steele, L. P., Mühle, J., Rigby, M., Salameh, P. K., Leist, M.,  
971 Krummel, P. B., Fraser, P. J., Weiss, R. F., and Prinn, R. G.: Atmospheric histories and growth  
972 trends of C<sub>4</sub>F<sub>10</sub>, C<sub>5</sub>F<sub>12</sub>, C<sub>6</sub>F<sub>14</sub>, C<sub>7</sub>F<sub>16</sub> and C<sub>8</sub>F<sub>18</sub>, *Atmos. Chem. Phys.*, 12, 9, 4313-4325,  
973 10.5194/acp-12-4313-2012, 2012.
- 974 Ji, L., Lu, S., Yang, J., Du, C., Chen, Z., Buekens, A., and Yan, J.: Municipal solid waste  
975 incineration in China and the issue of acidification: A review, *Waste Management & Research*,  
976 34, 4, 280-297, 10.1177/0734242x16633776, 2016.
- 977 Jianming, S.: Synthesis of Hexafluoropropene by Co-pyrolysis Reaction of Tetrafluoroethylene  
978 with Octafluorocyclobutane, Masters Degree, Department of Chemical Engineering, Zhajiang  
979 University, Hangzhou, China, 2006.

- 980 Jones, A. R., Thomson, D. J., Hort, M., and Devenish, B.: The UK Met Office's next-generation  
981 atmospheric dispersion model, NAME III, in: Air Pollution Modelling and Its Application XVII,  
982 edited by: Borrego, C., and Norman, A.-L., 580-589, 2007.
- 983 Kannan, G. K., Gupta, M., and Chandra Kapoor, J.: Estimation of gaseous products and  
984 particulate matter emission from garden biomass combustion in a simulation fire test chamber,  
985 Atmos. Environ., 39, 3, 563-573, 2005.
- 986 Kass, W.: Tracing Technique in Geohydrology, CRC Press, 1998.
- 987 Kim, J. H., Oh, C. H., Lee, N. E., and Yeom, G. Y.: Effect of  $N_2O$  to  $C_4F_8/O_2$  on global warming  
988 during silicon nitride plasma enhanced chemical vapor deposition (PECVD) chamber cleaning  
989 using a remote inductively coupled plasma source, Jpn. J. Appl. Phys. Part 2 - Lett., 41, 12B,  
990 L1495-L1498, 10.1143/jjap.41.11495, 2002.
- 991 Kokkoris, G., Goodyear, A., Cooke, M., and Gogolides, E.: A global model for  $C_4F_8$  plasmas  
992 coupling gas phase and wall surface reaction kinetics, J. Phys. D: Appl. Phys., 41, 19, 195211,  
993 10.1088/0022-3727/41/19/195211, 2008.
- 994 Langenfelds, R. L., Krummel, P. B., Fraser, P. J., Steele, L. P., Ward, J., and Somerville, N. T.:  
995 Archiving of Cape Grim air, Baseline Atmospheric Program Australia 2009-2010, Melbourne,  
996 Australia, 2014, edited by: Derek, N., Krummel, P. B., and Cleland, S. J., pp. 44-45, Australian  
997 Bureau of Meteorology and CSIRO Marine and Atmospheric Research.
- 998 Lewis, R. J., Sr.: Food additives handbook, Chapman & Hall, New York, 1989.
- 999 Liu, X., Wang, J., Wang, Y., Zhang, Z., and Xiao, D.: Analysis of the insulation characteristics of  
1000 c- $C_4F_8/CO_2$  gas mixtures by the Monte Carlo method, Journal of Physics D: Applied Physics, 41,  
1001 1, 015206, 2008.
- 1002 Lovelock, J. E.: Atmospheric Fluorine Compounds as Indicators of Air Movements, Nature, 230,  
1003 5293, 379-&, 1971.
- 1004 Lunt, M. F., Rigby, M., Ganesan, A. L., and Manning, A. J.: Estimation of trace gas fluxes with  
1005 objectively determined basis functions using reversible-jump Markov chain Monte Carlo, Geosci.  
1006 Model Dev., 9, 9, 3213-3229, 10.5194/gmd-9-3213-2016, 2016.
- 1007 Mackay, D., Shiu, W. Y., Ma, K. C., and Lee, S.: Handbook of Physical-Chemical Properties and  
1008 Environmental Fate for Organic Chemicals, 2006.
- 1009 Maione, M., Giostra, U., Arduini, J., Furlani, F., Graziosi, F., Lo Vullo, E., and Bonasoni, P.: Ten  
1010 years of continuous observations of stratospheric ozone depleting gases at Monte Cimone (Italy)  
1011 — Comments on the effectiveness of the Montreal Protocol from a regional perspective, Sci.  
1012 Total Environ., 445-446, 155-164, 10.1016/j.scitotenv.2012.12.056, 2013.
- 1013 Matsunaga, N., Hori, M., and Nagashima, A.: Mutual diffusion coefficients of halogenated-  
1014 hydrocarbon refrigerant-air systems, High Temp.-High Press, 25, 63-70, 1993.

- 1015 Matsunaga, N., Hori, M., and Nagashima, A.: Measurements of the mutual diffusion coefficients  
1016 of gases by the Taylor method, 7th report, measurements on the SF<sub>6</sub>-air, SF<sub>6</sub>-N<sub>2</sub>, SF<sub>6</sub>-O<sub>2</sub>, CFC12-  
1017 N<sub>2</sub>, CFC12-O<sub>2</sub>, HCFC22-N<sub>2</sub> and HCFC22-O<sub>2</sub> systems, *Trans. Jpn. Soc. Mech. Eng. B.*, 68, 550–  
1018 555, 2002.
- 1019 Matsunaga, N., Hori, M., and Nagashima, A.: Measurements of the mutual diffusion coefficients  
1020 of carbon tetrafluoride and methyl bromide in air, nitrogen and oxygen, *Proc. 26th Jpn. Symp.*  
1021 *Therm. Props.*, 26, 499–501, 2005.
- 1022 Metropolis, N., Rosenbluth, A. W., Rosenbluth, M. N., Teller, A. H., and Teller, E.: Equation of  
1023 State Calculations by Fast Computing Machines, *J. Chem. Phys.*, 21, 6, 1087-1092,  
1024 10.1063/1.1699114, 1953.
- 1025 Miller, B. R., Weiss, R. F., Salameh, P. K., Tanhua, T., Grealley, B. R., Mühle, J., and Simmonds,  
1026 P. G.: Medusa: A sample preconcentration and GC/MS detector system for in situ measurements  
1027 of atmospheric trace halocarbons, hydrocarbons, and sulfur compounds, *Anal. Chem.*, 80, 5,  
1028 1536-1545, 10.1021/ac702084k, 2008.
- 1029 Morisaki, S.: Simultaneous thermogravimetry-mass spectrometry and pyrolysis--gas  
1030 chromatography of fluorocarbon polymers, *Thermochimica Acta*, 25, 2, 171-183, 1978.
- 1031 Morris, R. A., Miller, T. M., Viggiano, A. A., Paulson, J. F., Solomon, S., and Reid, G.: Effects  
1032 of electron and ion reactions on atmospheric lifetimes of fully fluorinated compounds, *J.*  
1033 *Geophys. Res.*, 100, D1, 1287-1294, 1995.
- 1034 Mühle, J., Ganesan, A. L., Miller, B. R., Salameh, P. K., Harth, C. M., Grealley, B. R., Rigby, M.,  
1035 Porter, L. W., Steele, L. P., Trudinger, C. M., Krummel, P. B., O'Doherty, S., Fraser, P. J.,  
1036 Simmonds, P. G., Prinn, R. G., and Weiss, R. F.: Perfluorocarbons in the global atmosphere:  
1037 tetrafluoromethane, hexafluoroethane, and octafluoropropane, *Atmos. Chem. Phys.*, 10, 11, 5145-  
1038 5164, 10.5194/acp-10-5145-2010, 2010.
- 1039 Myhre, G., D. Shindell (Coordinating Lead Authors), Bréon, F.-M., Collins, W., Fuglestvedt, J.,  
1040 Huang, J., Koch, D., Lamarque, J.-F., Lee, D., Mendoza, B., Nakajima, T., Robock, A., Stephens,  
1041 G., Takemura, T., and Zhang, H.: Anthropogenic and Natural Radiative Forcing, in: *Climate*  
1042 *Change 2013: The Physical Science Basis. Contribution of Working Group I to the Fifth*  
1043 *Assessment Report of the Intergovernmental Panel on Climate Change, Chapter 8*, edited by:  
1044 Stocker, T. F., Qin, D., Plattner, G.-K., Tignor, M., Allen, S. K., Boschung, J., Nauels, A., Xia,  
1045 Y., Bex, V., and Midgley, P. M., Cambridge University Press, Cambridge, United Kingdom and  
1046 New York, NY, USA, 2013.
- 1047 O'Doherty, S., Simmonds, P. G., Cunnold, D. M., Wang, H. J., Sturrock, G. A., Fraser, P. J.,  
1048 Ryall, D., Derwent, R. G., Weiss, R. F., Salameh, P., Miller, B. R., and Prinn, R. G.: In situ  
1049 chloroform measurements at Advanced Global Atmospheric Gases Experiment atmospheric  
1050 research stations from 1994 to 1998, *J. Geophys. Res.*, 106, D17, 20429-20444, 2001.
- 1051 O'Doherty, S., Rigby, M., Mühle, J., Ivy, D. J., Miller, B. R., Young, D., Simmonds, P. G.,  
1052 Reimann, S., Vollmer, M. K., Krummel, P. B., Fraser, P. J., Steele, L. P., Dunse, B., Salameh, P.  
1053 K., Harth, C. M., Arnold, T., Weiss, R. F., Kim, J., Park, S., Li, S., Lunder, C., Hermansen, O.,  
1054 Schmidbauer, N., Zhou, L. X., Yao, B., Wang, R. H. J., Manning, A. J., and Prinn, R. G.: Global

- 1055 emissions of HFC-143a ( $\text{CH}_3\text{CF}_3$ ) and HFC-32 ( $\text{CH}_2\text{F}_2$ ) from in situ and air archive atmospheric  
1056 observations, *Atmos. Chem. Phys.*, 14, 17, 9249-9258, 10.5194/acp-14-9249-2014, 2014.
- 1057 Oram, D.: Trends of long-lived anthropogenic halocarbons in the Southern Hemisphere and  
1058 model calculations of global emissions, P.D. thesis, University of East Anglia, Norwich, U.K.,  
1059 1999.
- 1060 Oram, D. E., Mani, F. S., Laube, J. C., Newland, M. J., Reeves, C. E., Sturges, W. T., Penkett, S.  
1061 A., Brenninkmeijer, C. A. M., Röckmann, T., and Fraser, P. J.: Long-term tropospheric trend of  
1062 octafluorocyclobutane ( $\text{c-C}_4\text{F}_8$  or PFC-318), *Atmos. Chem. Phys.*, 12, 1, 261-269, 10.5194/acp-  
1063 12-261-2012, 2012.
- 1064 Prinn, R. G., Weiss, R. F., Fraser, P. J., Simmonds, P. G., Cunnold, D. M., Alyea, F. N.,  
1065 O'Doherty, S., Salameh, P., Miller, B. R., Huang, J., Wang, R. H. J., Hartley, D. E., Harth, C.,  
1066 Steele, L. P., Sturrock, G., Midgley, P. M., and McCulloch, A.: A history of chemically and  
1067 radiatively important gases in air deduced from ALE/GAGE/AGAGE, *J. Geophys. Res.*, 105,  
1068 D14, 17751-17792, 10.1029/2000jd900141, 2000.
- 1069 Prinn, R. G., Huang, J., Weiss, R. F., Cunnold, D. M., Fraser, P. J., Simmonds, P. G., McCulloch,  
1070 A., Harth, C., Salameh, P., O'Doherty, S., Wang, R. H. J., Porter, L., and Miller, B. R.: Evidence  
1071 for substantial variations of atmospheric hydroxyl radicals in the past two decades, *Science*, 292,  
1072 5523, 1882-1888, 2001.
- 1073 Prinn, R. G., Weiss, R. F., Arduini, J., Arnold, T., DeWitt, H. L., Fraser, P. J., Ganesan, A. L.,  
1074 Gasore, J., Harth, C. M., Hermansen, O., Kim, J., Krummel, P. B., Li, S., Loh, Z. M., Lunder, C.  
1075 R., Maione, M., Manning, A. J., Miller, B. R., Mitrevski, B., Mühle, J., O'Doherty, S., Park, S.,  
1076 Reimann, S., Rigby, M., Saito, T., Salameh, P. K., Schmidt, R., Simmonds, P. G., Steele, L. P.,  
1077 Vollmer, M. K., Wang, R. H., Yao, B., Yokouchi, Y., Young, D., and Zhou, L.: History of  
1078 chemically and radiatively important atmospheric gases from the Advanced Global Atmospheric  
1079 Gases Experiment (AGAGE), *Earth Syst. Sci. Data*, 10, 2, 985-1018, 10.5194/essd-10-985-2018,  
1080 2018.
- 1081 Raju, R., Kudo, D., Kubo, Y., Inaba, T., and Shindo, H.: Warming potential reduction of  $\text{C}_4\text{F}_8$   
1082 using inductively coupled plasma, *Japanese Journal of Applied Physics Part 1-Regular Papers*  
1083 *Short Notes & Review Papers*, 42, 1, 280-285, 10.1143/jjap.42.280, 2003.
- 1084 Ravishankara, A. R., Solomon, S., Turnipseed, A. A., and Warren, R. F.: Atmospheric lifetimes  
1085 of long-lived halogenated species, *Science*, 259, 5092, 194-199, 1993.
- 1086 Rigby, M., Ganesan, A. L., and Prinn, R. G.: Deriving emissions time series from sparse  
1087 atmospheric mole fractions, *J. Geophys. Res.*, 116, D8, D08306, 10.1029/2010jd015401, 2011.
- 1088 Rigby, M., Prinn, R. G., O'Doherty, S., Montzka, S. A., McCulloch, A., Harth, C. M., Mühle, J.,  
1089 Salameh, P. K., Weiss, R. F., Young, D., Simmonds, P. G., Hall, B. D., Dutton, G. S., Nance, D.,  
1090 Mondeel, D. J., Elkins, J. W., Krummel, P. B., Steele, L. P., and Fraser, P. J.: Re-evaluation of  
1091 the lifetimes of the major CFCs and  $\text{CH}_3\text{CCl}_3$  using atmospheric trends, *Atmos. Chem. Phys.*, 13,  
1092 5, 2691-2702, 10.5194/acp-13-2691-2013, 2013.

- 1093 Rigby, M., Prinn, R. G., O'Doherty, S., Miller, B. R., Ivy, D., Mühle, J., Harth, C. M., Salameh,  
1094 P. K., Arnold, T., Weiss, R. F., Krummel, P. B., Steele, L. P., Fraser, P. J., Young, D., and  
1095 Simmonds, P. G.: Recent and future trends in synthetic greenhouse gas radiative forcing,  
1096 *Geophys. Res. Lett.*, 41, 7, 2623-2630, 10.1002/2013gl059099, 2014.
- 1097 Saito, T., Yokouchi, Y., Stohl, A., Taguchi, S., and Mukai, H.: Large emissions of  
1098 perfluorocarbons in East Asia deduced from continuous atmospheric measurements, *Environ. Sci.*  
1099 *Technol.*, 44, 11, 4089-4095, 10.1021/es1001488, 2010.
- 1100 Sasaki, K., Kawai, Y., Suzuki, C., and Kadota, K.: Absolute density and reaction kinetics of  
1101 fluorine atoms in high-density c-C<sub>4</sub>F<sub>8</sub> plasmas, *Journal of Applied Physics*, 83, 12, 7482-7487,  
1102 1998.
- 1103 Say, D., Ganesan, A. L., Lunt, M. F., Rigby, M., O'Doherty, S., Harth, C., Manning, A. J.,  
1104 Krummel, P. B., and Bauguitte, S.: Emissions of CFCs, HCFCs and HFCs from India, *Atmos.*  
1105 *Chem. Phys. Discuss.*, 2019, 1-30, 10.5194/acp-2018-1146, 2019.
- 1106 Siegemund, G., Schwertfeger, W., Feiring, A., Smart, B., Behr, F., Vogel, H., McKusick, B., and  
1107 Kirsch, P.: Fluorine Compounds, Organic, in: *Ullmann's Encyclopedia of Industrial Chemistry*,  
1108 2016.
- 1109 Simmonds, P. G., Rigby, M., McCulloch, A., Vollmer, M. K., Henne, S., Mühle, J., O'Doherty,  
1110 S., Manning, A. J., Krummel, P. B., Fraser, P. J., Young, D., Weiss, R. F., Salameh, P. K., Harth,  
1111 C. M., Reimann, S., Trudinger, C. M., Steele, P., Wang, R. H. J., Ivy, D. J., Prinn, R. G.,  
1112 Mitrevski, B., and Etheridge, D. M.: Recent increases in the atmospheric growth rate and  
1113 emissions of HFC-23 (CHF<sub>3</sub>) and the link to HCFC-22 (CHClF<sub>2</sub>) production, *Atmos. Chem.*  
1114 *Phys.*, 18, 6, 4153-4169, 10.5194/acp-18-4153-2018, 2018.
- 1115 Smith, A. M., Levchenko, V. A., Etheridge, D. M., Lowe, D. C., Hua, Q., Trudinger, C. M.,  
1116 Zoppi, U., and Elcheikh, A.: In search of in-situ radiocarbon in Law Dome ice and firn, *Nuclear*  
1117 *Instruments and Methods in Physics Research Section B: Beam Interactions with Materials and*  
1118 *Atoms*, 172, 1-4, 610-622, 10.1016/S0168-583X(00)00280-9, 2000.
- 1119 Sowers, T., Bernard, S., Aballain, O., Chappellaz, J., Barnola, J.-M., and Marik, T.: Records of  
1120 the  $\delta^{13}\text{C}$  of atmospheric CH<sub>4</sub> over the last 2 centuries as recorded in Antarctic snow and ice,  
1121 *Global Biogeochem. Cycles*, 19, GB2002, 10.1029/2004GB002408, 2005.
- 1122 Stanley, K. M., Grant, A., O'Doherty, S., Young, D., Manning, A. J., Stavert, A. R., Spain, T. G.,  
1123 Salameh, P. K., Harth, C. M., Simmonds, P. G., Sturges, W. T., Oram, D. E., and Derwent, R. G.:  
1124 Greenhouse gas measurements from a UK network of tall towers: technical description and first  
1125 results, *Atmos. Meas. Tech.*, 11, 3, 1437-1458, 10.5194/amt-11-1437-2018, 2018.
- 1126 Stohl, A., Forster, C., Frank, A., Seibert, P., and Wotawa, G.: Technical note: The Lagrangian  
1127 particle dispersion model FLEXPART version 6.2, *Atmos. Chem. Phys.*, 5, 2461-2474, 2005.
- 1128 Stohl, A., Seibert, P., Arduini, J., Eckhardt, S., Fraser, P., Grealley, B. R., Lunder, C., Maione, M.,  
1129 Mühle, J., O'Doherty, S., Prinn, R. G., Reimann, S., Saito, T., Schmidbauer, N., Simmonds, P.  
1130 G., Vollmer, M. K., Weiss, R. F., and Yokouchi, Y.: An analytical inversion method for  
1131 determining regional and global emissions of greenhouse gases: Sensitivity studies and

- 1132 application to halocarbons, *Atmos. Chem. Phys.*, 9, 5, 1597-1620, 10.5194/acp-9-1597-2009,  
1133 2009.
- 1134 Sturges, W. T., Penkett, S. A., Lee, J. M., and Sturges, K. E.: Stratospheric distribution and  
1135 lifetime of halogenated hydrocarbons; Final report to the European Commission, Contract EV5V-  
1136 CT92-0078, University of East Anglia, Norwich, 1995.
- 1137 Sturges, W. T., Oram, D. E., Penkett, S. A., Fraser, P. J., and Engel, A.: Long-lived halogenated  
1138 compounds in the stratosphere, in: *Non-CO<sub>2</sub> Greenhouse Gases: Scientific Understanding,  
1139 Control, and Implementation*, edited by: van Ham, J., Baede, A. P. M., Meyer, L. A., and Ybema,  
1140 R., Kluwer Academic Publishers, The Netherlands, 239-240, 2000.
- 1141 Sturrock, G. A., Etheridge, D. M., Trudinger, C. M., Fraser, P. J., and Smith, A. M.: Atmospheric  
1142 histories of halocarbons from analysis of Antarctic firn air: Major Montreal Protocol species, *J.  
1143 Geophys. Res.*, 107, D24, 4765, 10.1029/2002JD002548, 2002.
- 1144 Tabereaux, A. T.: Anode Effects, PFCs, Global Warming, and the Aluminum-Industry, *J. Miner.  
1145 Met. Mater. Soc.*, 46, 11, 30-34, 1994.
- 1146 Travnicek, W.: A study of light halogenated hydrocarbons in stratospheric air samples using CG-  
1147 MS, diploma thesis, Dept. Jülich, Fachhochschule Aachen, Germany, Aachen, 1998.
- 1148 Trudinger, C. M., Enting, I. G., Etheridge, D. M., Francey, R. J., Levchenko, V. A., Steele, L. P.,  
1149 Raynaud, D., and Arnaud, L.: Modeling air movement and bubble trapping in firn, *J. Geophys.  
1150 Res.*, 102, D6, 6747-6763, 10.1029/96jd03382, 1997.
- 1151 Trudinger, C. M., Etheridge, D. M., Rayner, P. J., Enting, I. G., Sturrock, G. A., and Langenfelds,  
1152 R. L.: Reconstructing atmospheric histories from measurements of air composition in firn, *J.  
1153 Geophys. Res.*, 107, D24, 4780, 10.1029/2002JD002545, 2002.
- 1154 Trudinger, C. M., Enting, I. G., Rayner, P. J., Etheridge, D. M., Buizert, C., Rubino, M.,  
1155 Krummel, P. B., and Blunier, T.: How well do different tracers constrain the firn diffusivity  
1156 profile?, *Atmos. Chem. Phys.*, 13, 3, 1485-1510, 10.5194/acp-13-1485-2013, 2013.
- 1157 Trudinger, C. M., Fraser, P. J., Etheridge, D. M., Sturges, W. T., Vollmer, M. K., Rigby, M.,  
1158 Martinerie, P., Mühle, J., Worton, D. R., Krummel, P. B., Steele, L. P., Miller, B. R., Laube, J.,  
1159 Mani, F. S., Rayner, P. J., Harth, C. M., Witrant, E., Blunier, T., Schwander, J., O'Doherty, S.,  
1160 and Battle, M.: Atmospheric abundance and global emissions of perfluorocarbons CF<sub>4</sub>, C<sub>2</sub>F<sub>6</sub> and  
1161 C<sub>3</sub>F<sub>8</sub> since 1800 inferred from ice core, firn, air archive and in situ measurements, *Atmos. Chem.  
1162 Phys.*, 16, 18, 11733-11754, 10.5194/acp-16-11733-2016, 2016.
- 1163 Tsai, W. T.: Fate of Chloromethanes in the Atmospheric Environment: Implications for Human  
1164 Health, Ozone Formation and Depletion, and Global Warming Impacts, *Toxics*, 5, 4,  
1165 10.3390/toxics5040023, 2017.
- 1166 van der Walt, I. J., Neomagus, H. W. J. P., Nel, J. T., Bruinsma, O. S. L., and Crouse, P. L.: A  
1167 kinetic expression for the pyrolytic decomposition of polytetrafluoroethylene, *J. Fluor. Chem.*,  
1168 129, 4, 314-318, 10.1016/j.jfluchem.2008.01.003, 2008.



1169 Victor, D. G., and MacDonald, G. J.: A model for estimating future emissions of sulfur  
1170 hexafluoride and perfluorocarbons, *Climatic Change*, 42, 4, 633-662, 1999.

1171 Vollmer, M. K., Mühle, J., Trudinger, C. M., Rigby, M., Montzka, S. A., Harth, C. M., Miller, B.  
1172 R., Henne, S., Krummel, P. B., Hall, B. D., Young, D., Kim, J., Arduini, J., Wenger, A., Yao, B.,  
1173 Reimann, S., O'Doherty, S., Maione, M., Etheridge, D. M., Li, S., Verdonik, D. P., Park, S.,  
1174 Dutton, G., Steele, L. P., Lunder, C. R., Rhee, T. S., Hermansen, O., Schmidbauer, N., Wang, R.  
1175 H. J., Hill, M., Salameh, P. K., Langenfelds, R. L., Zhou, L., Blunier, T., Schwander, J., Elkins, J.  
1176 W., Butler, J. H., Simmonds, P. G., Weiss, R. F., Prinn, R. G., and Fraser, P. J. C. J. D.:  
1177 Atmospheric histories and global emissions of halons H-1211 (CBrClF<sub>2</sub>), H-1301 (CBrF<sub>3</sub>), and  
1178 H-2402 (CBrF<sub>2</sub>CBrF<sub>2</sub>), *J. Geophys. Res.*, 121, 7, 3663-3686, 10.1002/2015jd024488, 2016.

1179 Vollmer, M. K., Young, D., Trudinger, C. M., Mühle, J., Henne, S., Rigby, M., Park, S., Li, S.,  
1180 Guillevic, M., Mitrevski, B., Harth, C. M., Miller, B. R., Reimann, S., Yao, B., Steele, L. P.,  
1181 Wyss, S. A., Lunder, C. R., Arduini, J., McCulloch, A., Wu, S., Rhee, T. S., Wang, R. H. J.,  
1182 Salameh, P. K., Hermansen, O., Hill, M., Langenfelds, R. L., Ivy, D., O'Doherty, S., Krummel, P.  
1183 B., Maione, M., Etheridge, D. M., Zhou, L., Fraser, P. J., Prinn, R. G., Weiss, R. F., and  
1184 Simmonds, P. G.: Atmospheric histories and emissions of chlorofluorocarbons CFC-13 (CClF<sub>3</sub>),  
1185  $\Sigma$ CFC-114 (C<sub>2</sub>Cl<sub>2</sub>F<sub>4</sub>), and CFC-115 (C<sub>2</sub>ClF<sub>5</sub>), *Atmos. Chem. Phys.*, 18, 2, 979-1002,  
1186 10.5194/acp-18-979-2018, 2018.

1187 Vollmer, M. K., Bernard, F., Mitrevski, B., Steele, L. P., Trudinger, C. M., Reimann, S.,  
1188 Langenfelds, R. L., Krummel, P. B., Fraser, P. J., Etheridge, D. M., Curran, M. A. J., and  
1189 Burkholder, J. B.: Abundances, emissions, and loss processes of the long-lived and potent  
1190 greenhouse gas octafluorooxolane (octafluorotetrahydrofuran, c-C<sub>4</sub>F<sub>8</sub>O) in the atmosphere,  
1191 *Atmos. Chem. Phys.*, 19, 6, 3481-3492, 10.5194/acp-19-3481-2019, 2019.

1192 Walters, D. N., Williams, K. D., Boutle, I. A., Bushell, A. C., Edwards, J. M., Field, P. R., Lock,  
1193 A. P., Morcrette, C. J., Stratton, R. A., Wilkinson, J. M., Willett, M. R., Bellouin, N., Bodas-  
1194 Salcedo, A., Brooks, M. E., Copsey, D., Earnshaw, P. D., Hardiman, S. C., Harris, C. M., Levine,  
1195 R. C., MacLachlan, C., Manners, J. C., Martin, G. M., Milton, S. F., Palmer, M. D., Roberts, M.  
1196 J., Rodríguez, J. M., Tennant, W. J., and Vidale, P. L.: The Met Office Unified Model Global  
1197 Atmosphere 4.0 and JULES Global Land 4.0 configurations, *Geosci. Model Dev.*, 7, 1, 361-386,  
1198 10.5194/gmd-7-361-2014, 2014.

1199 Zhihong, W., Seidel, S., Kokorin, A., and Rand, S.: Chapter 3.6, PFC, HFC, SF<sub>6</sub> emissions from  
1200 semiconductor manufacturing, in: *IPCC Good Practice Guidance and Uncertainty Management in*  
1201 *National Greenhouse Gas Inventories*, IGES, Hayama, Japan, 2001.  
1202  
1203

1204 **Tables**

1205 **Table 1.** Availability of *c*-C<sub>4</sub>F<sub>8</sub> in situ, flask, firn, and aircraft air measurements, measurements sites, and instrumentation

Station/Site	Network	Lat.	Lon.	Medusa no.	Data availability*
Zeppelin (ZEP), Ny-Ålesund, Svalbard	AGAGE	78.9	11.9	19	09/2010–12/2017
NEEM08 firn, Greenland	–	77.5	-51.1	9	Extracted 07/2008
Summit13 firn, Greenland	–	72.7	-38.6	7	Extracted 05/2013
Mace Head (MHD), Ireland	AGAGE	53.3	-9.9	2	06/2010–12/2017
Tacolneston (TAC), United Kingdom	UK DECC/AGAGE	52.5	1.1	13	05/2013–12/2017
Jungfraujoch (JFJ), Switzerland	AGAGE	46.5	8.0	12	11/2008–12/2017
Monte Cimone (CMN), Italy	AGAGE/ICO-CV	44.2	10.7	ADS-GC/MS	05/2013–12/2017
Trinidad Head (THD), USA	AGAGE	41.0	-124.1	4	06/2010–12/2017
Shangdianzi (SDZ), China	AGAGE/CMA	40.7	117.1	17	05/2010–08/2012, 15/2015–04/2017, 09/2017–12/2017
Gosan (GSN), South Korea	AGAGE/KNU	33.3	126.2	10	06/2010–09/2016, 04/2017–09/2017, 12/2017–12/2017
La Jolla (SIO), USA	AGAGE	32.9	-117.3	1	11/2009–08/2013, 01/2014–12/2017
NH flasks	SIO & other	33–46	-72 – -124	7, 1, 9	10/1973–04/2016
Aircraft flask samples, India	FAAM/UoB	9–28	72–86	21	06/2016–07/2016
Ragged Point (RPB), Barbados	AGAGE	13.2	-59.4	5	06/2010–06/2014, 10/2014–12/2017
Cape Matatula (SMO), American Samoa	NOAA/AGAGE	-14.2	-170.6	6	08/2010–12/2017
Aspendale (ASA), Australia	AGAGE	-38.0	145.1	9	04–10/2010, 05–07/2011, 05/2015–12/2017
Cape Grim (CGO), Australia	AGAGE	-40.7	144.7	3	09/2010–12/2017
CGAA flasks, Australia	CSIRO/BoM	-40.7	144.7	9, 7	04/1978–12/2010
DSSW20K firn, Antarctica <sup>+</sup>	–	-66.7	112.8	7	Extracted 12/1997
SPO01 firn, Antarctica	–	-90.0	-119	9	Extracted 01/2001

1206 \*Shorter interruptions are excluded.

1207 AGAGE: Advanced Global Atmospheric Gases Experiment (Prinn et al., 2018).

1208 NEEM08: Firn air samples collected in 2008 at the Northern Greenland Eemian Ice Drilling Project, Greenland were collected by the University of Copenhagen,  
1209 Denmark, the NEEM consortium, and the Commonwealth Scientific and Industrial Research Organisation (CSIRO) (Buizert et al., 2012).  
1210 Summit13: Firn samples collected in 2013 near Summit station, Greenland by the University of Rochester and Oregon State University.  
1211 UK DECC: The Tacolneston (TAC) site is part of the UK Deriving Emissions linked to Climate Change network (Stanley et al., 2018).  
1212 DSSW20K: Firn samples collected in December 1997 at Dome Summit South West 20 km, Law Dome by CSIRO, the Australian Antarctic Division (AAD), and the  
1213 Australian Nuclear Science and Technology Organisation (ANSTO) (see Trudinger et al., 2016 and citations therein).  
1214 SPO01: Firn samples collected in 2001 at South Pole, Antarctica, by Bowdoin College, the National Oceanic and Atmospheric Administration (NOAA), the  
1215 University of Colorado and the National Science Foundation (NSF) (Aydin et al., 2004; Sowers et al., 2005).  
1216 ICO-OV: Measurements at the Italian Climate Observatory “O. Vittori” Monte Cimone (CMN) were performed with a commercial Adsorption-Desorption System  
1217 with gas chromatograph and mass spectrometer (ADS-GC/MS) (Maione et al., 2013).  
1218 CMA: China Meteorological Administration.  
1219 KNU: Kyungpook National University, South Korea.  
1220 SIO & other: Most archived northern hemispheric (NH) samples were collected by the Scripps Institution of Oceanography, La Jolla and measured on Medusa 7.  
1221 FAAM/UoB: Air samples over India and the Indian Ocean were taken aboard the UK’s FAAM (Facility for Airborne Atmospheric Measurements) BAe-146 research  
1222 aircraft and analyzed on Medusa 21 at University of Bristol (UoB) (Say et al., 2019).  
1223 CGAA: Cape Grim Air Archive samples were collected by the CSIRO Oceans and Atmosphere and the Bureau of Meteorology (BoM), Australia predominantly  
1224 measured on the Aspendale Medusa 9 at CSIRO (Langenfelds et al., 2014; Fraser et al., 2018).  
1225  
1226  
1227  
1228  
1229  
1230  
1231  
1232  
1233  
1234

1235 **Table 2.** Regional  $c\text{-C}_4\text{F}_8$  emissions derived for eastern Asia from Gosan measurements (NAME-HB inversion) and comparison to global emissions ( $\text{Gg yr}^{-1}$ ,  $\text{kt yr}^{-1}$ )

	Eastern China <sup>#</sup>	Western Japan <sup>#</sup>	South Korea	North Korea	Taiwan <sup>#</sup>	$\Sigma$ eastern Asia	Global <sup>+</sup>	Global - $\Sigma$ eastern Asia
2010	$0.30 \pm 0.07$	$0.02 \pm 0.01$	$0.019 \pm 0.008$	$0.008 \pm 0.004$	$0.008 \pm 0.005$	$0.36 \pm 0.07$	$1.40 \pm 0.11$	$1.04 \pm 0.13$
2011	$0.35 \pm 0.07$	$0.02 \pm 0.01$	$0.016 \pm 0.007$	$0.006 \pm 0.003$	$0.007 \pm 0.005$	$0.41 \pm 0.07$	$1.52 \pm 0.10$	$1.12 \pm 0.12$
2012	$0.41 \pm 0.06$	$0.02 \pm 0.01$	$0.009 \pm 0.005$	$0.004 \pm 0.002$	$0.010 \pm 0.008$	$0.45 \pm 0.06$	$1.61 \pm 0.08$	$1.16 \pm 0.10$
2013	$0.46 \pm 0.09$	$0.02 \pm 0.01$	$0.017 \pm 0.007$	$0.007 \pm 0.004$	$0.008 \pm 0.005$	$0.51 \pm 0.09$	$1.67 \pm 0.09$	$1.15 \pm 0.13$
2014	$0.54 \pm 0.06$	$0.03 \pm 0.01$	$0.039 \pm 0.009$	$0.009 \pm 0.004$	$0.009 \pm 0.006$	$0.62 \pm 0.06$	$1.76 \pm 0.09$	$1.14 \pm 0.11$
2015	$0.59 \pm 0.09$	$0.02 \pm 0.01$	$0.041 \pm 0.010$	$0.011 \pm 0.005$	$0.011 \pm 0.009$	$0.68 \pm 0.09$	$1.88 \pm 0.10$	$1.21 \pm 0.13$
2016	$0.67 \pm 0.12$	$0.02 \pm 0.01$	$0.022 \pm 0.010$	$0.009 \pm 0.005$	$0.009 \pm 0.006$	$0.73 \pm 0.12$	$2.06 \pm 0.10$	$1.33 \pm 0.16$
2017	$0.68 \pm 0.13$	$0.02 \pm 0.01$	$0.014 \pm 0.011$	$0.006 \pm 0.005$	$0.010 \pm 0.009$	$0.73 \pm 0.13$	$2.20 \pm 0.11$	$1.47 \pm 0.17$
	China	Japan	South Korea	North Korea	Taiwan	Sum		
a priori <sup>*</sup>	$0.42 \pm 0.05$	$0.09 \pm 0.01$	$0.032 \pm 0.002$	$0.010 \pm 0.001$	$0.009 \pm 0.001$	$0.56 \pm 0.05$		
	Eastern China	Western Japan						
a priori <sup>*</sup>	0.185	0.0294						

1236 <sup>+</sup>Global emissions are the average of the emissions determined by the CSIRO and the Bristol inversion in this work.

1237 <sup>#</sup>Eastern China contains the provinces Anhui, Beijing, Hebei, Henan, Jiangsu, Liaoning, Shandong, Shanghai, Shanxi, Tianjin and Zhejiang. Western Japan contains  
1238 the prefectures Chugoku, Kansai, Shikoku and Okawa and Kyushu. Due to the lower sensitivities of the inversion in western China, eastern Japan, and parts of  
1239 Taiwan, where potential source industries are located, we cannot exclude further emissions in these regions and therefore total emissions are probably larger.

1240 <sup>\*</sup>Saito et al. (2010) emission estimates based on atmospheric measurements from November 2007 to September 2009 were used as a priori information and were  
1241 spread for each country uniformly over the area of each country. The resulting a priori estimates for eastern China and western Japan are additionally listed for  
1242 comparison with the inversion results for these regions.

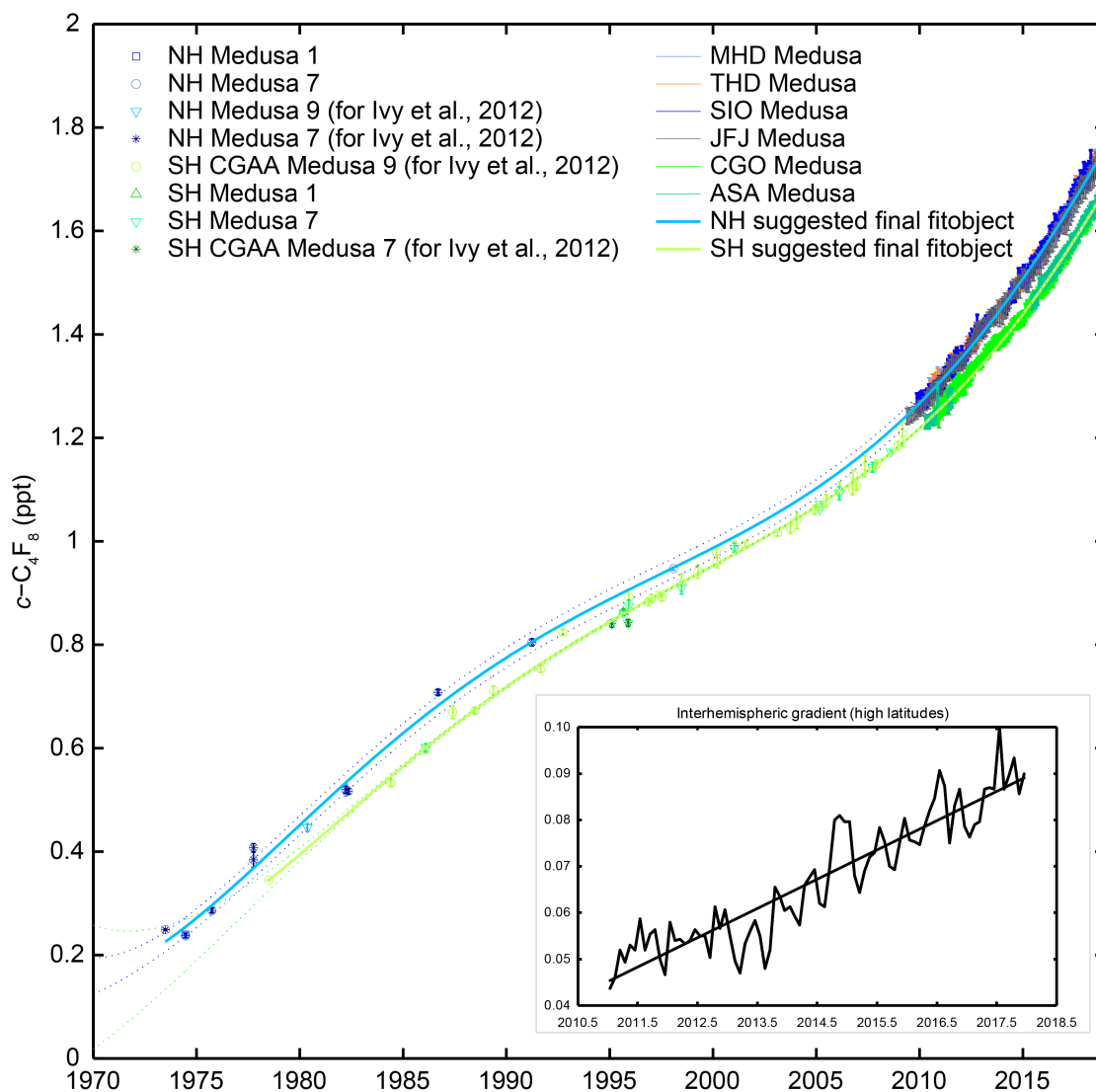
1243 Gosan measurements started in June 2010 with most complete coverages from 2011 to 2015.

1244

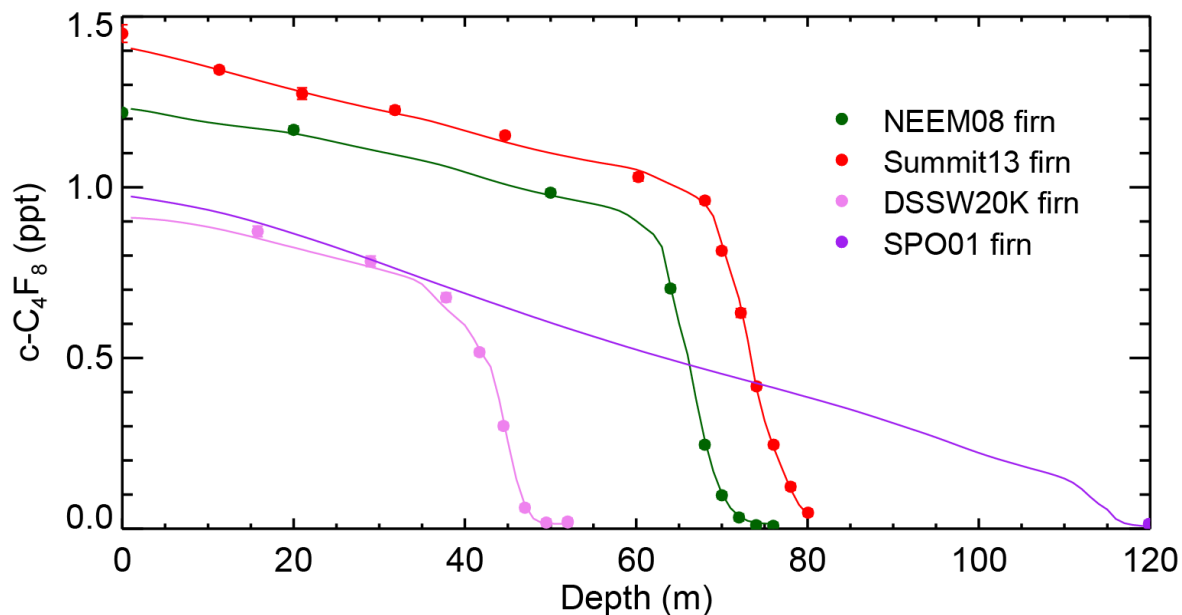
1245

1246

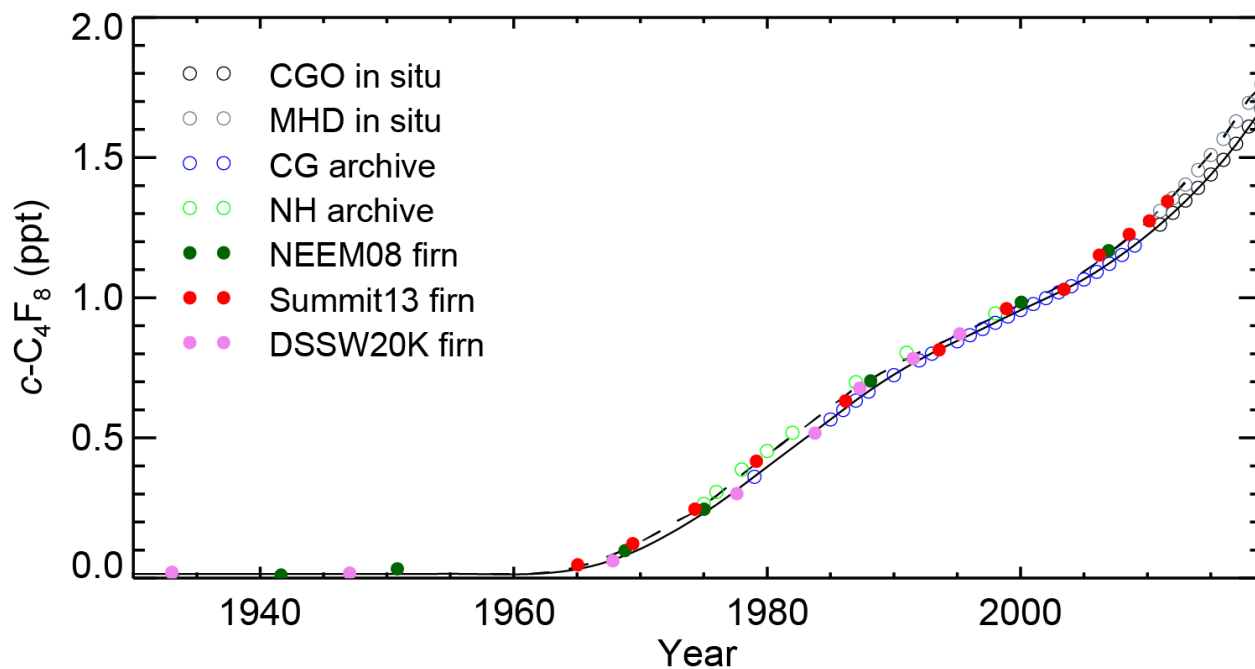
1247



1249  
 1250 **Figure 1.**  $c\text{-C}_4\text{F}_8$  mole fractions reconstructed from the late 1970s to 2018 from archived air samples and in situ  
 1251 measurements in both hemispheres. Cape Grim Air Archive (CGAA) and archived NH air samples are shown with  
 1252 symbols in shades of green and blue, respectively, reflecting different data subsets. For recent years, in situ  
 1253 measurements are shown as pollution removed monthly means for extra-tropical stations in the NH (MHD in light  
 1254 blue, THD in orange, SIO in darker blue, JFJ in grey) and in the SH (CGO in lighter green, ASA in pale green).  
 1255 Shown are the final data after an iterative filtering process described in the main text. The final suggested fits are  
 1256 shown as bold light green (SH) and bold light blue (NH) polynomial fits. Confidence bands ( $2\sigma$ ) are shown as dotted  
 1257 lines. Results for the tropical stations, RPB and SMO, the Asian stations, GSN and SDZ, and the Arctic station, ZEP,  
 1258 are omitted here for clarity. For individual samples, error bars reflect measurement precisions. For monthly means,  
 1259 error bars represent standard deviations. The inset shows the interhemispheric gradient from in situ measurements at  
 1260 high latitudes (MHD, THD, SIO, and CGO) from 2011 to 2017

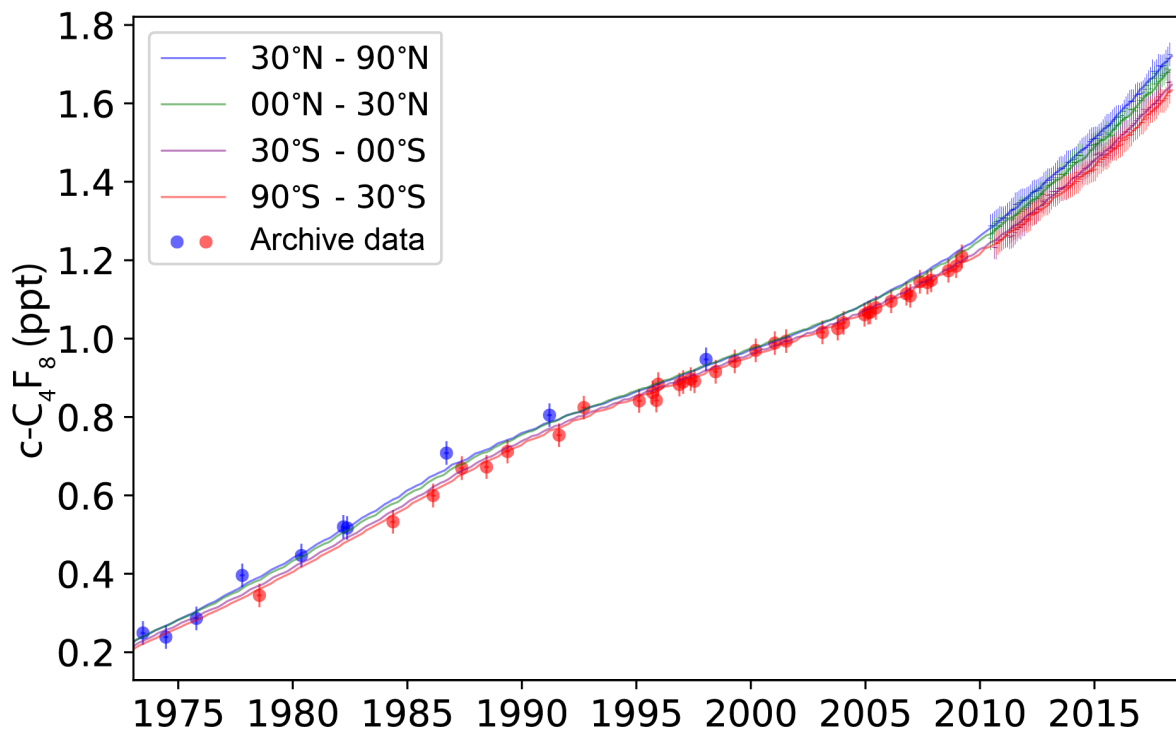


1261  
 1262 **Figure 2.** Depth profile of  $c\text{-C}_4\text{F}_8$  measured dry-air molar mole fractions (parts per trillion, ppt) in air extracted from  
 1263 polar firn at NEEM08 (Northern Greenland, dark green) and Summit13 (Greenland, red) in the NH and DSSW20K  
 1264 (Eastern Antarctica, pink) and SPO01 (South Pole, purple) in the SH, together with the simulated depth profiles for  
 1265 each site (dark green, red, pink, and purple lines) that correspond to the emissions inferred by the CSIRO inversion.  
 1266 The modelled depth profiles for each site (solid lines) are based on the inversion of measurements from all firn sites,  
 1267 archive, and in situ data. Measurement precisions ( $1\sigma$ ) are shown as error bars and are generally smaller than the  
 1268 plotting symbol.  
 1269



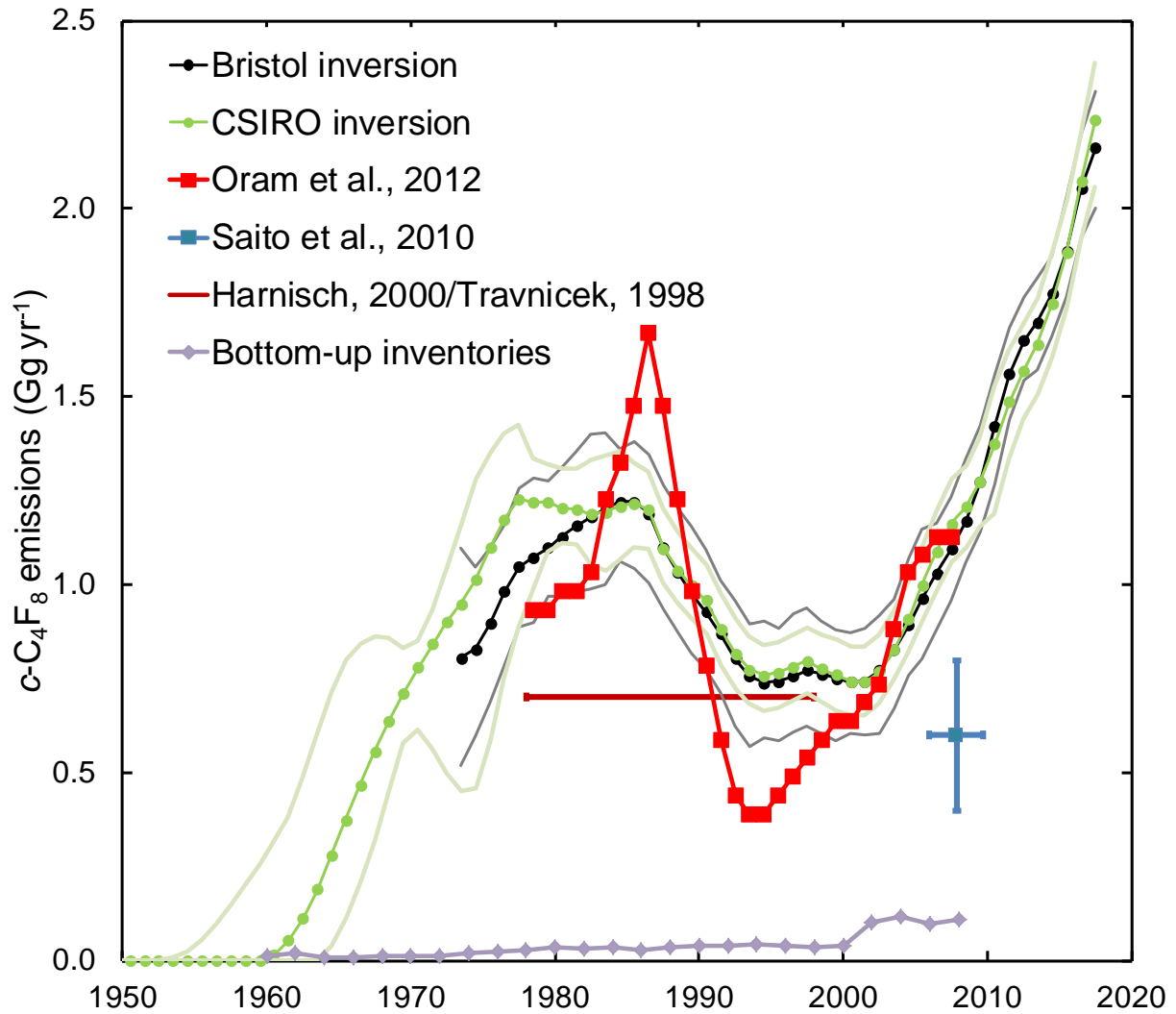
1270  
 1271 **Figure 3.** Historic atmospheric  $c\text{-C}_4\text{F}_8$  mole fractions reconstructed for the extra-tropical Northern and Southern  
 1272 Hemispheres from air extracted from polar firn (full circles, NEEM08 in dark green, Summit13 in red, DSSW20K in  
 38

1273 pink, against mean or effective ages; SPO01 with mean age of ~1890 is not shown), annual values from spline fits to  
 1274 Cape Grim Air Archive (CG archive, open blue circles) and in situ measurements at Cape Grim (CGO, open black  
 1275 circles), archived air samples (NH archive, open green circles) and in situ measurements at Mace Head (MHD, open  
 1276 grey circles). Also shown are reconstructed abundances based on optimized emissions determined by the CSIRO  
 1277 inversion for the extra-tropical SH (black line) and NH (dashed black line).  
 1278



1279  
 1280 **Figure 4.** Historic  $c\text{-C}_4\text{F}_8$  mole fractions from archive samples in both hemispheres (filled circles) and pollution-free  
 1281 monthly mean in situ data from AGAGE background sites (MHD and THD in blue, RPB in green, SMO in purple  
 1282 and CGO in green, vertical bars, bar size represents variability of monthly means) are shown together with the  
 1283 Bristol inversion results for the four latitudinal bands represented by these background sites (30° N–90° N, 0° N–30°  
 1284 N, 0° S–30° S and 30° S–90° S, solid lines of same color).

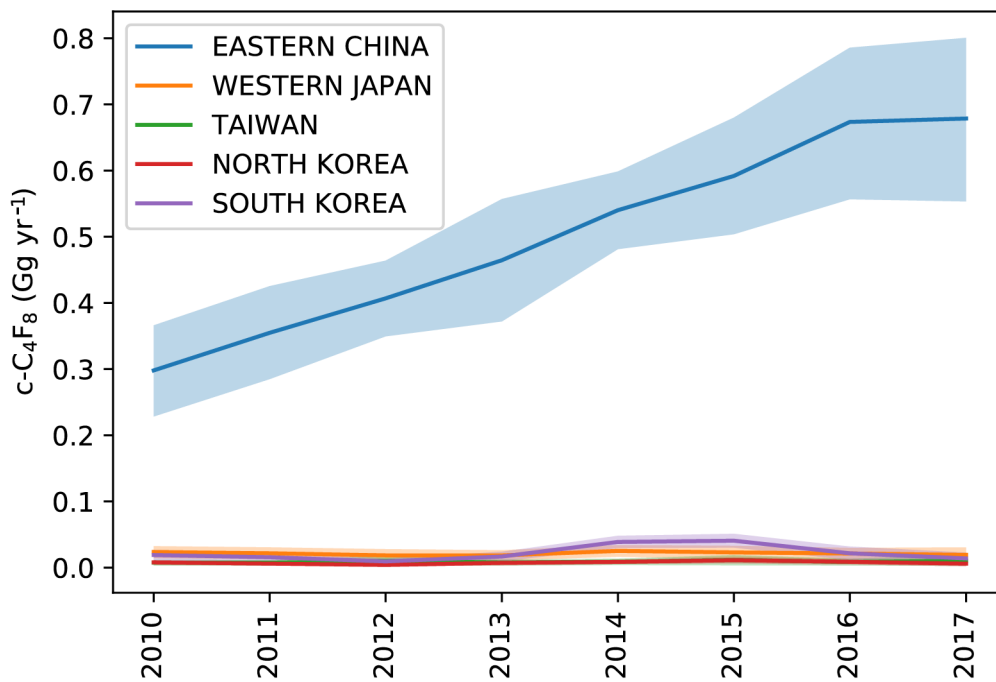
1285  
 1286  
 1287  
 1288  
 1289  
 1290  
 1291  
 1292



1293  
 1294 **Figure 5.** Global  $c\text{-C}_4\text{F}_8$  emissions reconstructed by the CSIRO inversion (green dots and line, light green  $2\sigma$   
 1295 uncertainty bands) from 1950 and by the Bristol inversion (black dots and line, grey  $1\sigma$  uncertainty bands) from the  
 1296 early 1970s to present. In situ and archive data are used in both inversions, while firm air data are only used in the  
 1297 CSIRO inversion. Emission estimates by Oram et al., 2012 (red), Saito et al., 2010 (blue), Harnisch, 2000/Travnicek,  
 1298 1998 (brown) and from available bottom-up inventory information (grey) are shown for comparison.

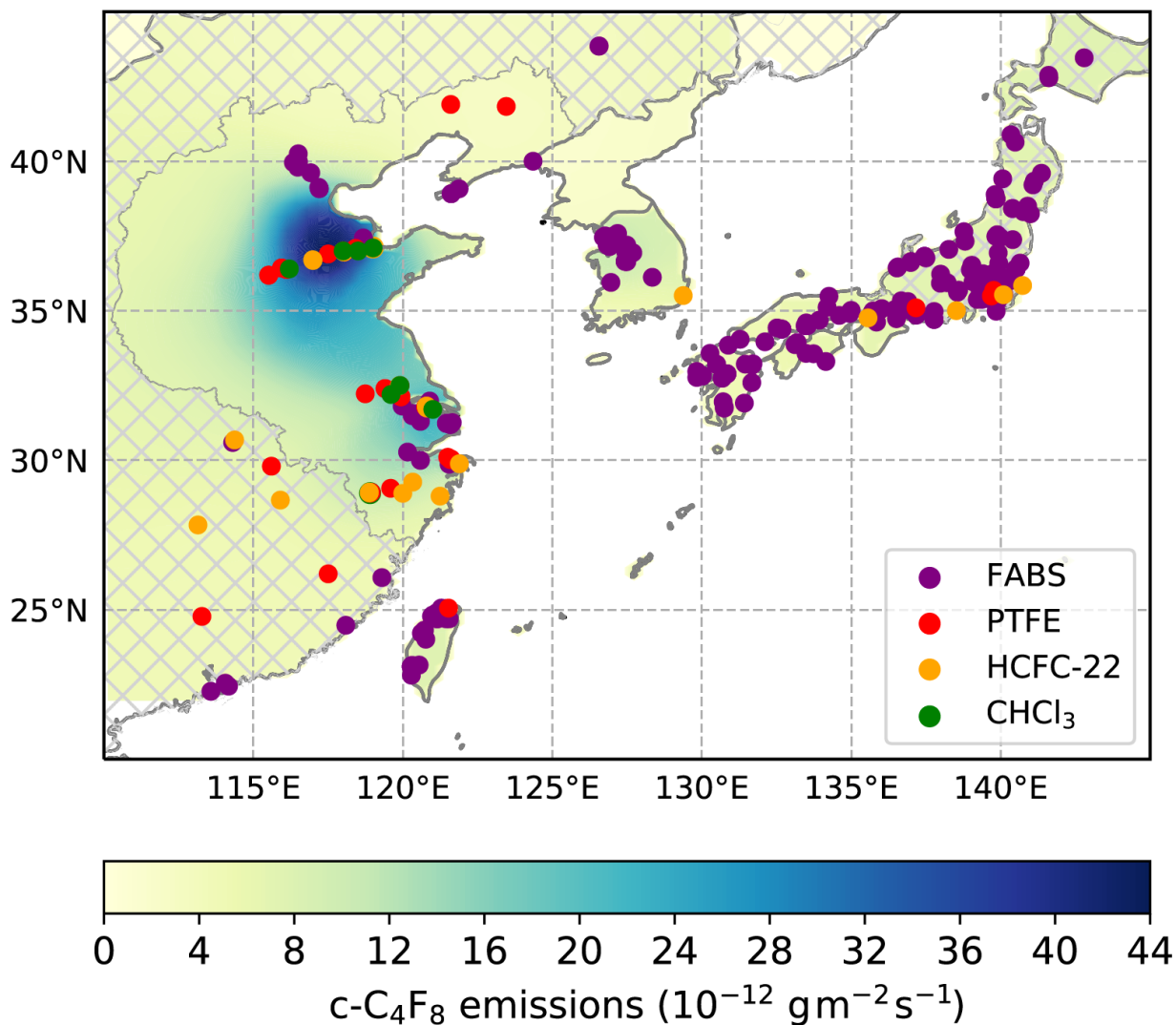
1299  
 1300  
 1301  
 1302  
 1303  
 1304  
 1305  
 1306  
 1307





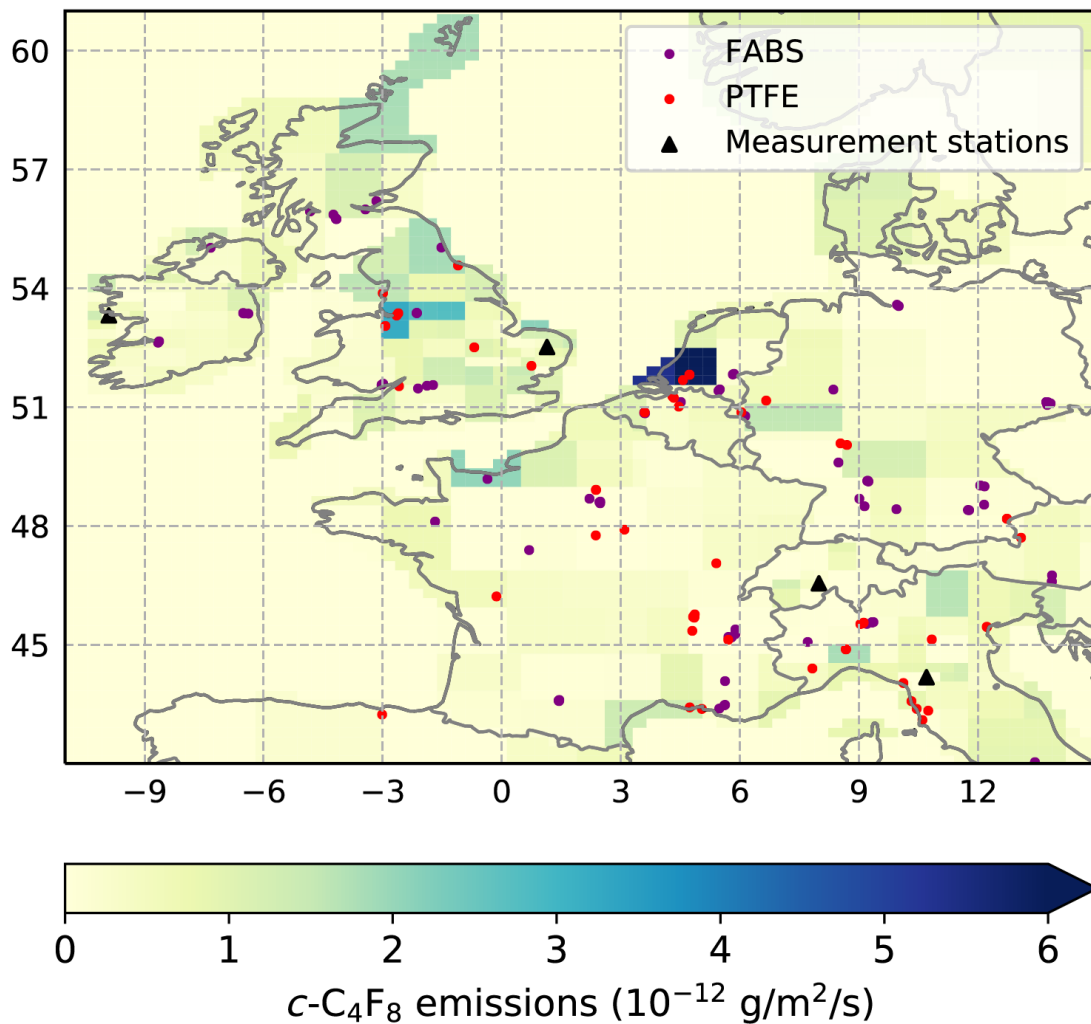
1308  
 1309 **Figure 6.** *c*-C<sub>4</sub>F<sub>8</sub> emission in eastern Asia as determined by the NAME-HB regional inversion of measurements at  
 1310 the Gosan station, Jeju Island, South Korea are dominated by emissions from eastern China (blue), followed by  
 1311 emissions from western Japan (orange). Emissions from South Korea (violet) are much smaller, but show a small  
 1312 maximum in 2014 and 2015. Emissions from Taiwan (green) and North Korea (red) also small. Shadings represent  
 1313 uncertainty bands of emissions.

1314  
 1315  
 1316  
 1317  
 1318  
 1319  
 1320  
 1321  
 1322  
 1323  
 1324  
 1325  
 1326  
 1327  
 1328  
 1329



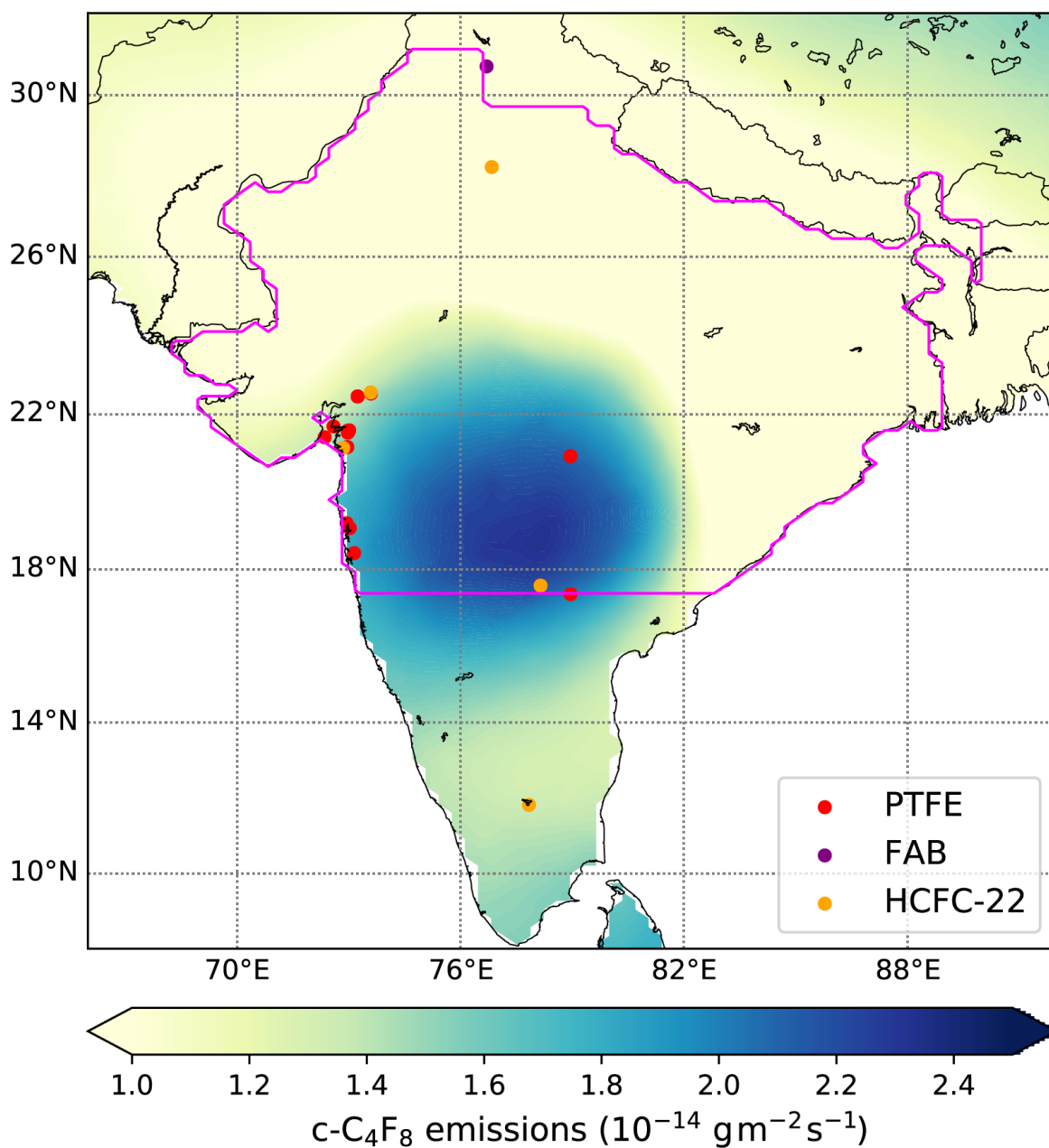
1330  
 1331 **Figure 7.** Mean  $c\text{-C}_4\text{F}_8$  emission strength (shades of green and blue,  $10^{-12} \text{ g m}^{-2} \text{ s}^{-1}$ ) in eastern Asia from 2010 to  
 1332 2017 determined by the NAME-HB inversion from measurements at the Gosan station, Jeju Island, South Korea.  
 1333 The hatching indicates areas for which emissions are not reported due to relatively low sensitivities of the inversion.  
 1334 Emissions predominantly occur in the densely industrialized Shandong, Tianjin and parts of Henan and Hebei  
 1335 provinces south/southwest of Beijing as well as in Shanghai and neighboring provinces Jiangsu (to the north), Anhui  
 1336 (to the west) and Zhejiang (to the south) of the Yangtze River Delta region. Shown are industries with potential  $c\text{-C}_4\text{F}_8$   
 1337 emissions: Semiconductor fabrication plants (FABS, purple dots,  
 1338 [en.wikipedia.org/wiki/List\\_of\\_semiconductor\\_fabrication\\_plants](https://en.wikipedia.org/wiki/List_of_semiconductor_fabrication_plants), [www.10stripe.com/featured/map/semiconductor-](http://www.10stripe.com/featured/map/semiconductor-fabs.php)  
 1339 [fabs.php](http://www.10stripe.com/featured/map/semiconductor-fabs.php) and other sources) and TFE/HFP/PTFE/FEP production facilities (PTFE, red dots,  
 1340 [www.qianzhan.com/analyst/detail/220/170629-c33a2ca7.html](http://www.qianzhan.com/analyst/detail/220/170629-c33a2ca7.html) and other sources). HCFC-22 (orange dots) and  
 1341 chloroform ( $\text{CHCl}_3$ , green dots) production facilities are shown as the TFE and HFP monomers needed to produce  
 1342 PTFE and FEP fluoropolymers are produced via pyrolysis of HCFC-22 and  $c\text{-C}_4\text{F}_8$  is an intermediate/by-product in  
 1343 this process, while HCFC-22 is manufactured from  $\text{CHCl}_3$ .

1344  
 1345



1346  
 1347 **Figure 8.** Mean  $c\text{-C}_4\text{F}_8$  emission strength (shades of green and blue,  $10^{-12} \text{ g m}^{-2} \text{ s}^{-1}$ ) in North Western Europe ( $42^\circ \text{ N}$   
 1348 to  $59^\circ \text{ N}$  and  $-11^\circ \text{ E}$  to  $15^\circ \text{ E}$ ) from 2013–2017 determined by the InTEM inversion from measurements at four sites  
 1349 (Mace Head, Ireland, Tacolneston, United Kingdom, Jungfrauoch, Switzerland, and Monte Cimone, Italy, black  
 1350 triangles). Also shown are potential industrial emitters of  $c\text{-C}_4\text{F}_8$ . Locations of potential TFE/HFP/PTFE/FEP  
 1351 production facilities (red dots) are based on company websites (3M, Chemours, Daikin, DuPont, Saint-Gobain, and  
 1352 Solvay) and are much less certain than the corresponding location information for eastern Asia. Also shown are  
 1353 semiconductor fabrication plants (purple dots, [en.wikipedia.org/wiki/List\\_of\\_semiconductor\\_fabrication\\_plants](http://en.wikipedia.org/wiki/List_of_semiconductor_fabrication_plants),  
 1354 [www.10stripe.com/featured/map/semiconductor-fabs.php](http://www.10stripe.com/featured/map/semiconductor-fabs.php), and other sources).

1355  
 1356  
 1357  
 1358  
 1359  
 1360  
 1361



1362  
 1363 **Figure 9.** Mean  $c\text{-C}_4\text{F}_8$  emission strength (shades of green and blue,  $10^{-14} \text{ g m}^{-2} \text{ s}^{-1}$ ) over the Indian subcontinent for  
 1364 June and July 2016 determined by the NAME-HB inversion based on air samples taken on-board UK's FAAM  
 1365 (Facility for Airborne Atmospheric Measurements) BAe-146 research aircraft. Also shown are the locations of one  
 1366 semiconductor fabrication plant (FAB, purple dot) and several potential TFE/HFP/PTFE/FEP production facilities  
 1367 (PTFE, red dots, Solvay/CYTEC, Hindustan Fluorocarbons, and Gujarat Fluorochemicals facilities) as potential  $c\text{-C}_4\text{F}_8$   
 1368 sources. HCFC-22 (orange dots) production facilities are also shown as the TFE and HFP monomers needed to  
 1369 produce PTFE and FEP fluoropolymers are produced via pyrolysis of HCFC-22 and  $c\text{-C}_4\text{F}_8$  is an intermediate/by-  
 1370 product in this process. The outline of the Northern and Central India (NCI) model domain is shown as a pink line.  
 1371